HHS Public Access

Author manuscript

Nat Immunol. Author manuscript; available in PMC 2014 December 16.

Published in final edited form as:

Nat Immunol. 2014 May ; 15(5): 457–464. doi:10.1038/ni.2867.

The AGC kinase serum- and glucocorticoid-regulated kinase 1 (SGK1) regulates T_H1 and T_H2 differentiation downstream of mTORC2

Emily B. Heikamp[1], **Chirag H. Patel**[1], **Sam Collins**[2], **Adam Waickman**[1], **Min-Hee Oh**[2], **Im-Hong Sun**[1], **Peter Illei**[3], **Archna Sharma**[4], **Aniko Naray-Fejes-Toth**[5], **Geza Fejes-Toth**[5], **Jyoti Sen**[4], **Maureen R. Horton**[2], and **Jonathan D. Powell**[1]

[1]Sidney Kimmel Comprehensive Cancer Research Center, Department of Oncology, Johns Hopkins University School of Medicine, Baltimore, MD 21231

[2]Department of Medicine, Johns Hopkins University School of Medicine, Baltimore, MD

[3]Department of Pathology, Johns Hopkins University School of Medicine, Baltimore, MD

[4]Lymphocyte Development Unit, Laboratory of Immunology, National Institute on Aging, National Institutes of Health, Baltimore, MD

[5]Dartmouth Medical School, Department of Physiology, Lebanon NH

Abstract

Serum- and glucocorticoid-regulated kinase 1 (SGK1) is an AGC kinase that regulates membrane sodium channel expression in renal tubular cells in an mTORC2-dependent manner. We hypothesized that SGK1 might represent a novel mTORC2-dependent regulator of T cell differentiation and function. Here we demonstrate that upon activation by mTORC2, SGK1 promoted T_H2 differentiation by negatively regulating the NEDD4-2 E3 ligase-mediated destruction of transcription factor JunB. Simultaneously, SGK1 repressed the production of interferon-γ (IFN-γ) by controlling the expression of the long isoform of transcription factor TCF-1. Consistent with these findings, mice with a selective deletion of SGK1 in T cells were resistant to experimentally induced asthma, generated robust amounts of IFN-γ in response to viral infections and more readily rejected tumors.

Correspondence should be addressed to J.D.P. (poweljo@jhmi.edu)., Phone 410-502-7887.

Author contributions: E.B.H. Helped design and perform experiments and write the paper.
J.D.P. Conceived of the project, helped design the experiments and write the paper.
M.R.H. Helped design the lung experiments and contributed to writing the paper.
C.H.P., S.C., M.H.O., I.H.S. assisted in performing the in vivo experiments and biochemistry.
A.W. contributed to the design of experiments and interpretation of data.
A.S. and J.S. Constructed the TCF1 plasmid.
A.N.F.T. and G.F.T. Generated the SGK1-floxed mice.
P.I. Scored the lung histology.

COMPETING FINANCIAL INTERESTS
The authors have no competing financial interests.

INTRODUCTION

AGC kinases are serine/threonine protein kinases that are broadly involved in regulating numerous aspects of cell physiology, including growth, survival and metabolism[1]. The serum- and glucocorticoid-regulated kinase 1 (SGK1) is an AGC kinase that is activated by sequential phosphorylation of two highly conserved regulatory motifs. The T-loop domain is phosphorylated at threonine 256 by the kinase PDK1 (ref. [2]), and the hydrophobic motif is phosphorylated at serine 422 by mTORC2 (refs. [3,4]). Compared to other AGC kinases that are also downstream of mTOR, such as Akt and S6 kinase, relatively little is known about SGK1. Downstream targets of SGK1 include E3 ubiquitin ligases such as NEDD4-2 (refs. [5,6]), transcription factors such as Foxo[7,8], and other kinases like GSK-3β[9]. In the kidney, SGK1 phosphorylates and inhibits NEDD4-2 to prevent degradation of the epithelial Na^+ channel, thus allowing sodium to be reclaimed in the urine when serum concentrations of sodium are low[5,10,11]. Recently, it has been shown that SGK1 mRNA is upregulated by sodium in lymphocytes, and that mice that are fed a high salt diet develop more severe T_H17-mediated autoimmune encephalomyelitis[12,13]. Loss of SGK1 in T cells leads to a selective defect in pathogenic T_H17 differentiation, due to decreased expression of the interleukin 23 (IL-23) receptor[12]. The role of SGK1 in other T cell lineages, however, has yet to be determined.

We became interested in SGK1 because it is a downstream target of mTOR, which serves as a critical node in a highly conserved signaling pathway that integrates multiple inputs from the environment[14,15]. In the immune system, mTOR integrates various signals, such as cytokines and costimulatory molecules, to influence T cell differentiation[15]. mTOR can associate with two distinct protein complexes (mTORC1 and mTORC2) to drive the selective differentiation of $CD4^+$ T cells. Genetic deletion of mTOR in $CD4^+$ T cells has shown that loss of both mTORC1 and mTORC2 signaling results in a default T regulatory (Treg) phenotype upon T cell activation[16,17]. Loss of either mTORC1 or mTORC2 leads to selective deficits in distinct T cell lineages. For example, genetic deletion of the mTORC2 adapter protein Rictor in $CD4^+$ T cells results in defective T_H2 differentiation, characterized by an inability to produce IL-4 (refs. [18,19]). Despite the critical role of mTOR in regulating T effector and Treg cell differentiation, the precise downstream targets of mTOR that control differentiation into distinct helper T cell subsets have yet to be elucidated.

Because SGK1 is a downstream target of mTORC2, we hypothesized that it might be involved in mTORC2 regulation of T_H2 lineage commitment. To this end, we generated mice in which SGK1 was selectively deleted in T cells by crossing *Sgk1*$^{fl/fl}$ mice[11] with *Cd4*-Cre expressing mice (hereafter referred to as T-*Sgk1*$^{-/-}$ mice). We show that loss of SGK1 led to decreased production of IL-4 and inappropriate release of interferon-γ (IFN-γ) under T_H2 polarizing conditions *in vitro*. In a mouse model of allergic asthma, we found that loss of SGK1 resulted in diminished T_H2 responses and protection against disease. Mechanistically, we show that SGK1 promoted T_H2 differentiation by preventing ubiquitination and destruction of the transcription factor JunB by NEDD4-2 and its adaptor protein Ndfip. Alternatively, we found that T-*Sgk1*$^{-/-}$ mice produced increased amounts of IFN-γ under T_H1 polarizing conditions *in vivo*, which was associated with both stronger anti-tumor and anti-viral immune responses. The ability of SGK1 to inhibit T_H1

differentiation was mediated in part by its ability to regulate the expression of the long isoform of TCF-1 via β-catenin and GSK-3β. Overall, our findings define distinct signaling pathways downstream of SGK1 that provide new evidence as to how mTOR controls helper T cell differentiation.

RESULTS

SGK1 is activated upon antigen recognition in T cells

Sgk1 RNA is expressed in resting naïve T cells (Supplementary Fig. 1a). We wanted to determine whether SGK1 is activated upon T cell stimulation by measuring the phosphorylation of the SGK1 substrate N-myc downregulated gene 1 (p-NDRG1 T346)[20]. Activation of T cells led to an increase in SGK1 activity (Fig. 1a). The kinetics of SGK1 activation paralleled the mTORC2-dependent activation of Akt (p-Akt S473). Next, we investigated whether SGK1 activity was modulated by polarizing cytokines upon T cell activation. Consistent with a recent report[12], SGK1 mRNA was expressed under all polarizing conditions *in vitro*, but expression was highest under T_H17 conditions (Supplementary Fig. 1b). Interestingly, we found that SGK1 activity was acutely induced to a similar degree under all polarizing conditions (Fig. 1b).

In light of the role of mTOR in regulating SGK1 activity in HEK293T, MCF-7 and HeLa cells[3,21], we sought to determine whether SGK1 was also activated in an mTOR-dependent manner in T cells (Supplementary Fig. 2a). Phosphorylation of NDRG1 increased upon T cell stimulation, but this effect was abrogated in the presence of the mTOR kinase inhibitor PP242 (Fig. 1c)[22]. Consistent with these results, inhibition of Akt phosphorylation (p-Akt S473) was also observed, indicating successful blockade of mTORC2 activity[23,24,25] (Fig. 1c). Likewise, the deletion of the mTORC2 component Rictor mitigated both Akt and SGK1 activation (Fig. 2a, Supplementary Fig. 2b,c). Having established that SGK1 signaling is mTORC2-dependent in T cells, we wanted to determine if SGK1 might function downstream of mTORC2 to regulate helper T cell differentiation. To address this question, mice were generated in which SGK1 was selectively deleted in T cells by breeding $Sgk1^{fl/fl}$ mice[11] with mice transgenic for Cre under control of the *Cd4* promoter and enhancer regions (T-$Sgk1^{-/-}$ mice) (Supplementary Fig. 1a). Upon stimulation, phosphorylation of NDRG1 was markedly decreased in T-$Sgk1^{-/-}$ $CD4^+$ T cells (Fig. 2a). Alternatively, the selective deletion of SGK1 in T cells did not affect Akt or S6 phosphorylation (Supplementary Fig. 2b,c).

The role of SGK1 in the maturation of peripheral T cells has never been described. Thymic development was essentially not different between wild-type and T-$Sgk1^{-/-}$ mice (Supplementary Fig. 3a) and there were no differences in the percent of $CD3^+$, $B220^+$, $CD4^+$ and $CD8^+$ cells in the spleen and lymph nodes compared to wild-type mice (Fig. 2b–e). Subtle differences in absolute T cell numbers and expression of activation markers were observed (Supplementary Fig. 3b–g). Finally there was a slight increase in $Foxp3^+$ T cells in the spleens of T-$Sgk1^{-/-}$ mice when compared to wild-type mice (6.23% vs 7.50%) however these differences were not observed in the lymph nodes (Supplementary Fig. 3h). T-$Sgk1^{-/-}$ $CD4^+$ T cells displayed a slightly reduced rate of proliferation (Fig. 2f). Nevertheless, T-$Sgk1^{-/-}$ $CD4^+$ T cells produce similar amounts of IL-2 compared to wild-type cells (Fig.

2g). Thus, the deletion of SGK1 does not greatly impact the composition of the peripheral T cell compartment.

SGK1 regulates T_H1 and T_H2 differentiation

In light of the ability of mTORC2 to regulate T_H2 generation[18,19], we wanted to determine whether loss of SGK1 affected T_H1 and T_H2 differentiation. $CD4^+$ T cells from wild-type and T-*Sgk1*$^{-/-}$ mice were polarized under T_H0, T_H1, or T_H2 conditions and interrogated for IL-4 production. As expected, wild-type T cells polarized under T_H2 conditions produced IL-4 upon re-challenge (Fig. 3a). However, T cells from T-*Sgk1*$^{-/-}$ mice failed to produce robust amounts of IL-4. Furthermore, loss of SGK1 resulted in decreased production of the T_H2 cytokines IL-5 and IL-13 (Fig. 3b,c).

Next, we examined the ability of T cells from T-*Sgk1*$^{-/-}$ mice to produce IFN-γ and to be polarized to T_H1 effector cells. Without any polarizing cytokines, T cells from C57BL/6 mice will preferentially differentiate into T_H1 cells (Fig. 3d). $CD4^+$ T cells from both wild-type and T-*Sgk1*$^{-/-}$ mice activated and cultured under non-polarizing (T_H0) or T_H1 polarizing conditions led to the generation of IFN-γ producing cells. However, T cells from T-*Sgk1*$^{-/-}$ mice robustly expressed IFN-γ even when they were differentiated under T_H2 conditions (Fig. 3d). Thus, T cells lacking SGK1 fail to produce IL-4, IL-5, and IL-13, but instead inappropriately produce IFN-γ under T_H2 polarizing conditions. Consistent with recent studies (ref. [12,13]), SGK1 does not affect T_H17 polarization (Supplementary Fig. 4).

Next, we examined the lineage-specific transcription factors T-bet and GATA-3. As expected, wild-type T cells cultured under T_H1 conditions expressed abundant T-bet, while cells cultured under T_H2 conditions robustly expressed GATA-3 (Fig. 3e). Alternatively, T cells derived from T-*Sgk1*$^{-/-}$ mice expressed abundant T-bet when cultured under either T_H1 or T_H2 conditions. Such cells also failed to express GATA-3 under T_H2 polarizing conditions. Overall, these observations demonstrate a role for SGK1 in reciprocally regulating T_H1 and T_H2 differentiation. During $CD4^+$ T cell effector differentiation, SGK1 activation simultaneously enhances IL-4 production and inhibits IFN-γ production.

SGK1 regulates T_H2 differentiation by stabilizing JunB

We sought to define a biochemical mechanism by which SGK1 regulates T_H1 and T_H2 differentiation. We did not observe a defect in IL-4 receptor expression or IL-4-induced STAT6 phosphorylation in the absence of SGK1 (*data not shown*). Previous studies on the role of SGK1 in renal epithelial cells have demonstrated that SGK1 negatively regulates the HECT-type E3 ligase by phosphorylation at serine 342 and serine 448 (refs. [5,10]). A closely related homolog of NEDD4-2 is the ubiquitin ligase Itch, which has been shown to interact with the NEDD4 family–interacting protein 1 (Ndfip1) adapter protein to mediate polyubiquitination of JunB[26,27]. JunB has been shown to be essential for T_H2 development[26,28]. We sought to determine if the defect in T_H2 differentiation that we observed in T-*Sgk1*$^{-/-}$ mice could be in part due to increased ubiquitination and destruction of JunB by NEDD4-2. As previously shown[28], JunB abundance was higher in wild-type T cells cultured under T_H2 conditions compared to those cultured under T_H1 conditions (Fig. 4a). In SGK1-deficient T cells, we observed that JunB protein abundance was decreased

under both T_H1 and T_H2 polarizing conditions (Fig. 4a). These findings correlated with the phosphorylation status of NEDD4-2 at S342. That is, inhibition of NEDD4-2 (as measured by p-NEDD4-2 S342) was greatest under T_H2 conditions and decreased in the absence of SGK1 (Fig. 4a).

We next investigated the ability of SGK1 to regulate NEDD4-2 *in vivo*. To this end, we adoptively transferred congenically marked Thy1.1$^+$, ovalbumin (OVA)-specific CD4$^+$ T cells from wild-type or T-*Sgk1*$^{-/-}$ mice into naïve hosts that were subsequently immunized with OVA in alum to induce a T_H2 response. Similar to the *in* vitro results, we observed p-NEDD4-2 S342 phosphorylation and inhibition upon stimulation of wild-type adoptively transferred cells (Fig. 4b). By contrast, NEDD4-2 was not phosphorylated and inhibited in T-*Sgk1*$^{-/-}$ adoptively transferred cells.

Our data are consistent with the hypothesis that NEDD4-2 degrades JunB protein in T cells lacking SGK1 even under T_H2 conditions, both *in vitro* and *in vivo*. To further test this hypothesis, wild-type and T-*Sgk1*$^{-/-}$ T CD4$^+$ cells were activated under T_H2 conditions in the presence of the proteasome inhibitor MG132. JunB abundance was markedly decreased in the T cells lacking SGK1 when compared to the wild-type T cells (Fig. 4c). However, expression of JunB protein was restored in T-*Sgk1*$^{-/-}$ cells in the presence of MG132, suggesting that Jun B is expressed in T-*Sgk1*$^{-/-}$ T cells but is subsequently degraded. To confirm that JunB degradation was due to increased ubiquitination we immunoprecipitated JunB in wild-type and T-*Sgk1*$^{-/-}$ CD4+ T cells and immunoblotted for ubiquitin. We found that JunB was not ubiquitinated under T_H2 conditions in wild-type cells, but JunB ubiquitination was markedly enhanced in the absence of SGK1 (Fig. 4d).

Next, we wanted to determine whether we could rescue the ability of T-*Sgk1*$^{-/-}$ CD4$^+$ T cells to make IL-4 under T_H2 conditions by knocking down NEDD4-2 or Ndfip using siRNA. Knocking down either NEDD4-2 or Ndfip led to partial rescue of IL-4 production in the T-*Sgk1*$^{-/-}$ T_H2 polarized T cells (Fig. 4e). Knockdown was confirmed by measuring the expression of NEDD4-2 and Ndfip mRNA (Supplementary Fig. 5a,b). Additionally, NEDD4-2 knockdown was confirmed at the protein level, which correlated with the re-accumulation of JunB protein (Fig. 4f). It was difficult to confirm knockdown of Ndfip at the protein level because the available antibodies are not robust, however knockdown of Ndfip also resulted in the re-accumulation of JunB protein (*data not shown*). Altogether, these results suggest that SGK1 activation promotes T_H2 differentiation in part by negatively regulating E3 ligases that target JunB for destruction.

T-*Sgk1*$^{-/-}$ mice are resistant to Th2-mediated asthma

Since we had defined the role of SGK1 in regulating the differentiation of helper T cells *in vitro*, we wanted to confirm this paradigm in an *in vivo* model. We chose to study the OVA-alum allergic asthma model because T_H2 cells are involved in the early pathogenesis of this disease[29]. Therefore, we hypothesized that T-*Sgk1*$^{-/-}$ mice would be resistant to allergic asthma. Wild-type mice mounted a stereotypic T_H2 response to this allergic stimulus, characterized by IL-4 in bronchoalveolar lavage (BAL) and IgE in serum. However, BAL and serum from T-*Sgk1*$^{-/-}$ mice contained significantly less IL-4 and IgE (Supplementary Fig. 6a,b). Alternatively, we detected OVA-specific IgG2a, characteristic of a T_H1 response

in the serum of T-*Sgk1*$^{-/-}$ mice (Supplementary Fig. 6c). Along these lines, lung lymphocytes from T-*Sgk1*$^{-/-}$ mice inappropriately produced IFN-γ when stimulated *ex vivo* (Supplementary Fig. 6d). Thus in this *in vivo* model of T_H2-mediated inflammation, loss of SGK1 in T cells abrogated the T_H2 response and instead produced an inappropriate T_H1 response to an allergic stimulus.

In light of these findings we wanted to determine if deleting SGK1 in T cells could prevent allergen-induced lung pathology. To this end we challenged wild-type and T-*Sgk1*$^{-/-}$ mice with house dust mite (HDM) extract. Similar to our findings in the OVA-alum adjuvant model, we observed a marked decrease in the T_H2 response of T-*Sgk1*$^{-/-}$ mice when challenged with HDM extract. Expression of IL-4, IL-13 and IL-5 in the lungs of T-*Sgk1*$^{-/-}$ mice was markedly diminished when compared to wild-type mice (Fig. 5a–c). Likewise, we observed a decrease in the expression of these cytokines by $CD4^+$ T cells in the mediastinal lymph nodes of T-*Sgk1*$^{-/-}$ mice (Fig. 5d–g). We observed a significant decrease in the absolute number of $CD4^+$ T cells in the lymph nodes of T-*Sgk1*$^{-/-}$ mice, however, the there was no significant decrease observed in the lungs and BAL fluid between wild-type and T-*Sgk1*$^{-/-}$ mice (Supplementary Fig. 6e,f). Consistent with our model, $CD4^+$ T cells in the lungs, BAL and lymph nodes of T-*Sgk1*$^{-/-}$ mice produced significantly more IFN-γ compared to wild-type mice (Fig. 5h,i). Furthermore, the T-*Sgk1*$^{-/-}$ mice displayed decreased total IgE, in addition to decreased HDM-specific IgE and IgG1 (Fig. 5j–l). Finally, the lungs of the T-*Sgk1*$^{-/-}$ mice demonstrated markedly decreased goblet cell hyperplasia and decreased peribronchiolar and perivascular inflammation when compared to the lungs of the wild-type mice (Fig. 5m–q). Thus, loss of SGK1 in T cell protects against allergen-induced T_H2-mediated lung disease.

SGK1 negatively regulates IFN-γ production via TCF-1

The SGK1–NEDD4-2–Ndfip–JunB axis provides a selective mechanism as to why T-*Sgk1*$^{-/-}$ $CD4^+$ T cells do not differentiate towards a T_H2 phenotype. However, it does not adequately explain why $CD4^+$ T cells produce IFN-γ under T_H2 conditions in the absence of SGK1. It has previously been reported that the glycogen synthase kinase-3β (GSK-3β) is inhibited by the AGC kinases Akt and SGK1 (ref. [9]). In turn, GSK-3β phosphorylates β-catenin and targets this protein for degradation[30,31]. We observed a marked decrease in expression of β-catenin in T-*Sgk1*$^{-/-}$ T cells (Fig. 6a). β-catenin is critical during T_H2 differentiation because it promotes early GATA-3 expression by binding at the proximal promoter[32]. In the absence of SGK1, GSK-3β remains highly active and thus there is very little total β-catenin. On the other hand, inhibiting GSK-3β in the T-*Sgk1*$^{-/-}$ T cells with LiCl leads to an increase in total β-catenin (Fig. 6a).

The transcription factor T cell factor 1 (TCF-1) is both a downstream target of β-catenin and a transcriptional co-activator with β-catenin[31–33]. Similar to T-*Sgk1*$^{-/-}$ mice, mice deficient in TCF-1 produce more IFN-γ even under T_H2 polarizing conditions[32]. Specifically, the long isoforms of TCF-1 contain an additional β-catenin binding domain, and these long isoforms promote T_H2 polarization by increasing expression of GATA-3 and repressing expression of IFN-γ[32]. We hypothesized that there would be decreased expression of the long form of TCF-1 in the T cells lacking SGK1. Wild-type and T-*Sgk1*$^{-/-}$ $CD4^+$ T cells

were polarized under T_H1 and T_H2 conditions and assayed for TCF-1 protein. We found that the long isoforms of TCF-1 were decreased in T-*Sgk1*$^{-/-}$ under both T_H1 and T_H2 polarizing conditions, but there was no difference in expression of the short isoforms of this protein (Fig. 6b).

To determine if SGK1 regulates TCF-1 expression at the transcriptional level, we designed primers that flank the β-catenin binding domain to specifically detect the long isoform of TCF-1. In the absence of SGK1, we observed decreased transcription of the long isoforms of TCF-1 at 72 h post-TCR activation, and a complete absence of transcripts at 8 days post-stimulation (Fig. 6c). To further test this hypothesis, we sought to rescue the phenotype of T-*Sgk1*$^{-/-}$ CD4$^+$ T cells by retroviral transduction with a vector encoding the long isoform of TCF-1 (FL-TCF-1) and a human CD8 reporter (Fig. 6d). We sorted transduced cells for human CD8, then restimulated the cells and assayed for the production of IFN-γ by intracellular staining. Wild-type T cells polarized under T_H2 conditions failed to express IFN-γ. T cells from the T-*Sgk1*$^{-/-}$ mice, transduced with the empty vector (EV), expressed significant amounts of IFN-γ under T_H2 conditions. Alternatively, IFN-γ expression was mitigated when the T-*Sgk1*$^{-/-}$ T cells were transfected with FL-TCF-1 (Fig. 6d). These data support a model whereby under T_H2 conditions SGK1 inhibits the GSK-3β-mediated degradation of β-catenin, leading in turn to increased expression of the long form of TCF-1 and inhibition of IFN-γ (Supplementary Fig. 7).

T-*Sgk1*$^{-/-}$ mice mount robust T_H1-mediated immune responses

The ability of SGK1 to regulate T_H2 responses is in part due to its ability to negatively regulate IFN-γ. We wondered whether we would also see an increase in IFN-γ *in vivo* under strongly polarizing T_H1 conditions in the T-*Sgk1*$^{-/-}$ mice. To this end, congenically marked Thy1.1$^+$, OVA-specific wild-type and T-*Sgk1*$^{-/-}$ CD4$^+$ T cells were adoptively transferred into Thy1.2$^+$ wild-type mice that were infected intravenously with OVA-expressing vaccinia virus (Vac-OVA) which induces robust T_H1 immune responses. Vaccinia infection led to a marked increase in the numbers of OVA-specific IFN-γ producing cells from wild-type mice. However, the T_H1 response by the T cells from the *Sgk1*$^{-/-}$ mice demonstrated an increase in both the percentage of IFN-γ producing cells and the amount of IFN-γ produced on a per cell basis (Fig. 7a). To confirm this observation, we challenged wild-type and T-*Sgk1*$^{-/-}$ mice with the PR8 strain of influenza virus, which also promotes a strong T_H1-mediated immune response. Similar to what we observed for vaccinia virus, CD4$^+$ T cells from T-*Sgk1*$^{-/-}$ mice produced more IFN-γ in response to influenza virus infection compared to wild-type mice (Fig. 7b).

To further assess the T_H1 response by T-*Sgk1*$^{-/-}$ cells *in vivo* we employed a model of T_H1-mediated tumor rejection, since T_H1-polarized CD4$^+$ T cells have previously been shown to have an important role in anti-tumor immunity[34]. To address this hypothesis, we injected wild-type and T-*Sgk1*$^{-/-}$ mice with 2×10^5 B16 melanoma cells intravenously, and harvested lungs 21 days later. Loss of SGK1 in T cells resulted in less than half as many lung tumors as compared to wild-type mice (Fig. 7c, Supplementary Fig. 8). While it is quite possible that the decrease in tumor burden could have been promoted by CD8$^+$ T cells, it is clear that the more effective response by the T-*Sgk1*$^{-/-}$ mice was associated with an increase

in $CD4^+$ IFN-γ producing T cells in the lungs (Fig. 7d). Next, we sought to further boost tumor immunity in T-*Sgk1*$^{-/-}$ mice by vaccination. Mice were immunized with vaccinia virus expressing OVA seven days prior to intravenous injection of B16 melanoma cells expressing OVA, and survival was monitored as the primary outcome. We found that T-*Sgk1*$^{-/-}$ mice had significantly prolonged survival compared to wild-type mice in response to a tumor vaccine (Fig. 7e). Thus, the targeted deletion of SGK1 in T cells leads to enhanced tumor immunity, characterized by more IFN-γ production and robust immunologic rejection of tumors.

DISCUSSION

A critical task of both the adaptive and innate immune system is to integrate cues from the immune microenvironment and then respond appropriately. Recently, it has become clear that the evolutionarily conserved serine/threonine kinase mTOR plays a central role in this process[15]. The outcome of mTOR activation is determined by the regulation of selective downstream signaling pathways and substrates. To this end, we have identified the AGC kinase SGK1 as an mTORC2 activated substrate that selectively regulates T_H1 and T_H2 helper T cell differentiation. T cells lacking SGK1 demonstrate a markedly diminished ability to differentiate into T_H2 cells both *in vitro* and *in vivo*. Furthermore, under T_H2 polarizing conditions the T-*Sgk1*$^{-/-}$ T cells inappropriately produced IFN-©. Thus, under T_H2 conditions SGK1 simultaneously promotes T_H2 differentiation while also inhibiting the production of T_H1 cytokines. Likewise, *in vivo* we observed increased IFN-© production by the T-*Sgk1*$^{-/-}$ T cells in the setting of viral infection and anti-tumor immunity. Of note, under T_H1 polarizing conditions *in vitro*, the T-*Sgk1*$^{-/-}$ cells produced equivalent levels of IFN-© as wild-type T cells. Perhaps this indicates that under strongly polarizing conditions *in vitro*, the ability of SGK1 to inhibit the T_H1 response is inconsequential. However, *in vivo*, under inflammatory conditions that predominantly favor T_H1 polarization, SGK1 signaling appears to limit the magnitude of the T_H1 immune response.

Our studies provide a mechanism by which mTOR (specifically mTORC2) activation regulates T_H1 and T_H2 differentiation. Recently, it has been reported that SGK1 plays a role in promoting the stability of pathogenic T_H17 cells[12]. Notably, in this study, as in ours, T_H17 differentiation was similar in both wild-type and T-*Sgk1*$^{-/-}$ T cells. However, it was shown that SGK1 plays a role in controlling the expression of the IL-23 receptor. As a result, T cells lacking SGK1 respond poorly to IL-23 and T-*Sgk1*$^{-/-}$ mice are resistant to the development of experimental autoimmune encephalitis (EAE). Furthermore, it was shown that an increase in the extracellular concentration of sodium leads to increased IL-23-mediated T_H17 differentiation and that this effect was abrogated in T-*Sgk1*$^{-/-}$ T cells. This report and another link these findings to the ability of increased dietary salt to exacerbate EAE[12,13].

Previous studies on the role of SGK1 in the kidney provided clues as to how this AGC kinase may be functioning in T cells[11]. In order to reclaim sodium in the urine, SGK1 prevents degradation of sodium channels by phosphorylating and inhibiting the NEDD4-2 E3 ubiquitin ligase[5,6]. Similarly, we found that SGK1 promoted T_H2 differentiation by phosphorylating and inhibiting NEDD4-2, thus preventing degradation of JunB. These

findings are consistent with previous reports that mice lacking Ndfip or Itch display a hyper-T_H2 phenotype[26,27]. In these studies loss of Ndfip or Itch led to accumulation of JunB and increased expression of IL-4. Overall, our studies serve to strengthen the link between mTOR-SGK1 and the regulation of cellular differentiation and function by E3-ligases. Just as these connections have been shown to be important in T cells and renal epithelial cells, we propose that these pathways will prove to be important for a diversity of cellular functions.

Our findings identify SGK1 as a potential target for the treatment of T_H2-mediated autoimmune and allergic diseases, such as asthma. Currently, non-specific immunosuppressive agents such as steroids play an important role in the treatment of acute asthma flares as well as in preventing recurrences[35–37]. Our data suggest that the selective inhibition of SGK1 might represent an immunomodulatory approach to treating and preventing the sequelae of asthma and other allergic diseases without globally inhibiting the immune system. Interestingly, small molecule inhibitors of SGK1 have already been developed[38,39]. Additionally, inhibiting SGK1 may be of therapeutic value in terms of enhancing T_H1-mediated immune responses, for example, in the setting of viral infections or as an adjunct to tumor immunotherapy. That is, while an asthmatic might take an SGK1 inhibitor to prevent the development of T_H2-mediated inflammation, the same small molecule inhibitor might be given to a patient in the midst of receiving cancer immunotherapy in order to enhance the anti-tumor response.

Methods

Mice

Mice were kept in accordance with guidelines of the Johns Hopkins University Institutional Animal Care and Use Committee. Mice with *lox*P-flanked *Sgk1* alleles were described previously[11], and mice with *lox*P-flanked *Rictor* alleles were provided by M. Magnuson[40]. C57BL/6, *Cd4*-Cre and OT-II mice were obtained from Jackson Laboratories and bred to Thy-1.1 backgrounds. 5C.C7 mice were from Taconic Farms.

Antibodies and reagents

The following antibodies for flow cytometry were from BD Biosciences: anti-B220 (RA3-6B2), anti-CD3 (2C11), anti-CD4 (RM4–5), anti-CD8 (Ly-3), anti-CD25 (PC61), anti-CD44 (IM7), anti-CD124 (mIL4R-M1), anti-IFN-γ (XMG1.2), anti-IL-17a (TC11-18H10), and anti-human CD8 (RPA-T8). Anti-CD62L (MEL-14), anti-IL-13 (eBio13A), anti-IL-5 (TRFK5), anti-T-bet (eBio4B10) and anti-Foxp3 (FJK-16s) were from eBioscience.

The following antibodies for immunoblotting were from Cell Signaling Technologies: Antibody to Rictor (2140), NDRG1 phosphorylated at Thr346 (5482), total NDRG1 (9408), antibody to Akt phosphorylated at S473 (4060), pan-Akt (4685), NEDD4-2 phosphorylated at Ser342 (4080), total NEDD4-2 (4013), TCF-1 (2206), antibody to β-catenin (9562), antibody to phosphorylated β-catenin (9561), antibody to phosphorylated STAT6 (9361). Anti-T-bet (4B10) and anti-GATA-3 (TWAJ) were from eBioscience. Anti-JunB (210) was

from Santa Cruz Biotechnology. Anti-ubiquitin was and actin were from Sigma. MG132 was from Sigma, PP242 was from Calbiochem, and CFSE was from Invitrogen.

T cell stimulation and polarization

$CD4^+$ T cells were purified by negative selection using a $CD4^+$ isolation kit and MACS Cell Separation (Miltenyi Biotec). For polarizing experiments, T cells were stimulated with irradiated autologous APCs or with plate-bound anti-CD3 and soluble anti-CD28. For APC-free stimulations, flat-bottomed plates were coated with anti-CD3 (3 μg/ml) diluted in PBS, and soluble anti-CD28 (2 μg/ml) was added to the cultures. For stimulation with APCs, T cells were cultured with irradiated APCs and anti-CD3 (1 μg/ml), followed by rest and expansion for 5 days. For rechallenge, live cells were harvested by Ficoll gradient, washed, and then stimulated with plate-bound anti-CD3 (1 μg/ml) and soluble anti-CD28 (2 μg/ml). Polarizing conditions were as follows: T_H0, anti-IL-4 (5 μg/ml) and anti-IFN-γ (5 μg/ml), with IL-2 (1 ng/ml) during the rest period; T_H1, IL-12 (5 ng/ml), IFN-γ (100 ng/ml) and anti-IL-4 (5 μg/ml), with IL-2 (1 ng/ml) during the rest period; T_H2, IL-4 (10 ng/ml), anti-IL-12 (5 μg/ml) and anti-IFN-γ (5 μg/ml), with IL-2 (1 ng/ml) during the rest period; T_H17, IL-6 (30 ng/ml), TGF-β (3 ng/ml), anti-IFN-γ (5 μg/ml), anti-IL-4 (5 μg/ml), and IL-23 (10 ng/ml) during the rest period. Stimulatory anti-CD3 (2C11) and anti-CD28 (37.51), as well as neutralizing anti-IFN-γ (XMG1.2) and anti-IL-4 (11B11) were purified from hybridoma supernatants prepared in-house. Neutralizing anti-IL-12p40 (C17.8) was from eBioscience. Cytokines were from Peprotech.

Adoptive transfer

1×10^6 naïve $CD4^+$ T cells specific for the OVA MHC class II epitope (OVA aa329–337) congenically marked with Thy1.1 were transferred intravenously to Thy1.2 C57BL/6 recipients by retro orbital injection. 1×10^6 pfu Vac-OVA was simultaneously administered by either retro orbital injection or intraperitoneal injection.

House Dust Mite Asthma Model

On days 0 and 7, mice were primed by intraperitoneal injection of 10 μg of house dust mite (HDM) extract (*D. pteronyssinus*, Greer Labs) in PBS. On days 14 and 21, mice were challenged via inhalation of 50 μg HDM extract per nostril. On day 24, mice are sacrificed for analysis. Lymphocytes from bronchoalveolar lavage (BAL) and mediastinal lymph nodes were stimulated *ex vivo* with PMA (phorbol 12-myristate 13-acetate) and ionomycin for 4 h. Lung lymphocytes were stimulated *ex vivo* with 30 μg HDM extract for 72 h, and supernatant from cultures were analyzed by ELISA. Differential cellular analysis of BAL was done via cytospin and Diff-quick staining. For histological analysis, lungs were formalin fixed, embedded in paraffin, and stained with hematoxylin and eosin, or periodic acid-Schiff (PAS), and scored by previously reported methods[41]. Peribronchiolar and perivascular inflammation was determined by a semi-quantitatively graded scale from 0–3, where a score of 0 = absent inflammation, 1 = mild, 2 = moderate, 3 = severe. Goblet cell hyperplasia was assessed by PAS staining of histologic sections, and was semi-quantitatively graded on a scale from 0–3, where a score of 0 = no or rare PAS-positive cells, 1 = less than 10% PAS-positive cells observed at 10×, 2 = between 10% and 25%

PAS-positive cells observed at 10×, and 3 = greater than 25% PAS-positive cells observed at 4×. A composite score was determined by multiplying the graded score and the percent of airways or vessels that exhibited a given pathological finding. All scoring was performed by a pathologist (P. Illei), who was blinded to the identity of the samples, and all slides were examined in a random order.

Influenza Model

On day 0, mice were challenged with intranasal influenza strain PR8 (Charles River) by injecting 600 egg infective dose (EID) per nostril for a final dose of 1200 EID. On day 8, mice were sacrificed. Lymphocytes from the lung were harvested by gentle mechanical and chemical digestion of lung parenchyma with collagenase and DNAse and stimulated *ex vivo* with PMA and ionomycin for 4 h. Experimental samples from groups were excluded from the final analysis if flow analysis of T lymphocytes from lungs demonstrated more than 70% $CD44^{-}$ and no detectable MHC class I or class II NP tetramer-positive cells, suggesting inadequate influenza inoculation.

B16 melanoma model

Mice were injected with 2×10^5 B16-OVA cells intravenously on day 0 and lungs were harvested 21 days later. Lung lymphocytes were stimulated *ex vivo* with PMA and ionomycin (Sigma) at a concentration of 50 ng/ml and 500 ng/ml, respectively. For survival experiments, mice were injected with 1×10^6 pfu VAC-OVA intraperitoneally on day 0, followed by intravenous injection with 2×10^5 B16-OVA cells on day 7.

Ovalbumin (OVA) airway sensitization model

OVA (Sigma-Aldrich) was adsorbed by gentle shaking for 30 min onto Imject Alum adjuvant (Pierce) to a final concentration of 250 μg/ml. Mice were primed by intraperitoneal injection of 50 μg of OVA-Alum in 200 μl. On day 7, mice were boosted by the same protocol. On days 15, 16, and 17, mice were challenged with intranasal OVA by injecting 25 μg OVA in PBS per nostril. On day 18, mice were sacrificed.

Intracellular staining

Brefeldin A (GolgiPlug; BD Biosciences) or monensin (GolgiStop; BD Biosciences) was used for cytokine staining. Cell were stained for surface antigens, fixed and made permeable with either the BD Cytofix/Cytoperm or the eBioscience Fixation/Permeabilization kit, then stained for intracellular cytokines. For intracellular staining of phosphorylated proteins, cells were fixed with 2.0% formalin and permeabilized with methanol.

Flow Cytometric Analysis

Flow cytometric data was acquired using a BD FACS Calibur or LSR II, and analyzed using FlowJo7.6 (Tree Star Inc, Ashland, OR). Gates were determined by using unstimulated controls or isotype controls where appropriate. Cells were sorted using a BD FACS Aria at the Flow Cytometry Core at the Sidney Kimmel Comprehensive Cancer Center, JHMI.

Immunoblot analysis

For immunoblot analysis of mTOR substrates, $CD4^+$ T cells were stimulated in regular medium with anti-CD3 (1 μg/ml), anti-CD28 (2 μg/ml) and antibody to hamster immunoglobulin IgG1 (0.75 μg/ml; G94-56; BD Biosciences). T cells were harvested by centrifugation and resuspended in ice-cold lysis buffer (20 mM Tris (pH 7.5), 150 mM NaCl, 1 mM EDTA, 1 mM EGTA, 1% Triton X-100, 2.5 mM sodium pyrophosphate, 1 mM β-glycerolphosphate (glycerol-2-phosphate), 1 mM sodium orthovanadate, 1 mM PMSF, 1× protease inhibitors (Roche) and lysed at 4 °C for 30 min. Lysates were cleared of debris by high-speed centrifugation. Equal protein mass from each condition was mixed with 4× LDS buffer (Invitrogen) and boiled for 10 min. Lysates were then loaded into NuPAGE gels (10% Bis–Tris gels, Invitrogen) and run at 150 V for 90 min. Protein was transferred to polyvinylidene fluoride (PVDF) membranes with transfer buffer (1× NuPAGE Transfer Buffer (Invitrogen) with 20% methanol) at 30 V for 90 min. Membranes were blocked in 5% nonfat dry milk (NFDM) for 60 min, washed briefly with Tris-buffered saline (pH=8) + 0.1% Tween-20 (TBST) and probed with primary antibody in 4% bovine serum albumin in TBST overnight at 4 °C. Membranes were washed with TBST three times for 10 min and probed with secondary antibody conjugated to horseradish peroxidase (HRP) in NFDM. Membranes were washed 2 times in TBST for 5 min, and then once in Tris-buffered saline once for 5 min. Enhanced chemiluminescent plus substrate (GE Healthcare) was used to detect HRP-labeled antibodies. Blots were developed using a Biospectrum Multispectrum Imaging System and images were acquired and analyzed using VisionWorks, LS Image Acquisition and Analysis software (UVP).

Enzyme-linked immunosorbent assay

IL-2, IL-4, IL-5, and IL-13 were analyzed by enzyme-linked immunosorbent assay as described by the manufacturer (eBioscience). Total serum IgE was measured using the following reagents from BD: anti-mouse IgE capture antibody (553413), mouse IgE standard (557080), and anti-mouse IgE biotinylated detection antibody (553419). HDM and OVA-specific antibodies were analyzed by enzyme-linked immunosorbent assay in Nunc-Immuno plates which had been coated overnight at 4 °C with 100 μl HDM (25 μg/ml in PBS) or OVA (20 μg/ml in PBS) and blocked for 1 h at 25 °C with assay diluent (eBioscience). Wells were washed several times and mouse serum samples diluted in assay diluent were added for 2 h or overnight. Wells were washed and then biotinylated anti-mouse immunoglobulin IgG1a (553441; BD) or IgG2a (553455; BD) diluted to a concentration of 0.5 μg/ml in assay diluent was added for 1 h. Wells were washed and then streptavidin-conjugated HRP (eBioscience) was added for 30 min. Wells were washed seven times, and then incubated for 15 min with tetramethylbenzidine substrate, or until the reaction approached saturation. Linear regression analysis or absorbance levels were used to determine antibody titers or relative differences.

Real-time PCR

RNA was isolated and reverse transcribed into cDNA using the SuperScript III First-Strand Synthesis System for RT-PCR (Invitrogen) according to the manufacturer’s protocol. Primers for short and long isoforms of TCF-1 were from Sigma, and primers to detect

NEDD4-2 and Ndfip were from Applied Biosystems. Primers used to detect TCF-1 long isoforms were the following: 5′-caatctgctcatgccctacc-3′ (forward) and 5′-gcctgtgaactccttgcttc-3′ (reverse). Relative amounts of long and short isoforms were quantified using real-time PCR with a SYBR green fluorescent probe (Applied Biosystems). Quantitative RT-PCR was performed using a Step One Plus Real Time PCR System (Applied Biosystems).

Retroviral transduction

T cells were stimulated with plate-bound anti-CD3 and soluble anti-CD28 (as described above) overnight prior to spinfection with supernatants from 293T Phoenix cells. The Phoenix helper-free retroviral ecotropic packaging cell line (Nolan Laboratory) was transfected using Lipofectamine 2000 (Invitrogen) with plasmids encoding MSCV retrovirus containing full-length TCF-1 and a human CD8 reporter. MSCV constructs were provided by J. Sen.

siRNA knockdown

T cells were stimulated with plate-bound anti-CD3 and soluble anti-CD28 (as described above) for 48 h prior to transfection. ON-TARGET siRNA reagents for scrambled control and NEDD4-2 and Ndfip specific RNA-mediated interference were from Dharmacon. Nucleofection reagents were from Lonza.

Statistical analysis

Prism version 5.0 (GraphPad Software) was used to perform statistical analyses, including unpaired Student's *t*-test, 2-way Analysis of Variance (ANOVA), and Log-rank (Mantel Cox) survival analysis. A P-value <0.05 was considered to be statistically significant.

Supplementary Material

Refer to Web version on PubMed Central for supplementary material.

Acknowledgments

We thank D. Pardoll, C. Gamper and members of the Powell Lab for helpful discussions. We thank the Magnuson lab for *Rictor*$^{-/-}$ mice. This work was supported by NIH grants R01 AI77610 (J.D.P.), DK 41481 (A.N.F.T.) and DK 58898 (G.F.T.). American Asthma Foundation Senior investigator award (J.D.P.) and the American Medical Association Seed Foundation Grant (E.B.H.).

References

1. Pearce LR, Komander D, Alessi DR. The nuts and bolts of AGC protein kinases. Nat Rev Mol Cell Biol. 2010; 11:9–22. 10.1038/nrm2822 nrm2822 [pii]. [PubMed: 20027184]
2. Biondi RM, Kieloch A, Currie RA, Deak M, Alessi DR. The PIF-binding pocket in PDK1 is essential for activation of S6K and SGK, but not PKB. EMBO J. 2001; 20:4380–4390.10.1093/emboj/20.16.4380 [PubMed: 11500365]
3. Garcia-Martinez JM, Alessi DR. mTOR complex 2 (mTORC2) controls hydrophobic motif phosphorylation and activation of serum- and glucocorticoid-induced protein kinase 1 (SGK1). Biochem J. 2008; 416:375–385. BJ20081668 [pii] 10.1042/BJ20081668. [PubMed: 18925875]
4. Yan L, Mieulet V, Lamb RF. mTORC2 is the hydrophobic motif kinase for SGK1. Biochem J. 2008; 416:19–21. BJ20082202 [pii] 10.1042/BJ20082202.

5. Debonneville C, et al. Phosphorylation of Nedd4-2 by Sgk1 regulates epithelial Na(+) channel cell surface expression. EMBO J. 2001; 20:7052–7059.10.1093/emboj/20.24.7052 [PubMed: 11742982]
6. Ichimura T, et al. 14-3-3 proteins modulate the expression of epithelial Na+ channels by phosphorylation-dependent interaction with Nedd4-2 ubiquitin ligase. J Biol Chem. 2005; 280:13187–13194. M412884200 [pii] 10.1074/jbc.M412884200. [PubMed: 15677482]
7. Di Pietro N, et al. Serum- and glucocorticoid-inducible kinase 1 (SGK1) regulates adipocyte differentiation via forkhead box O1. Mol Endocrinol. 2010; 24:370–380. me.2009-0265 [pii] 10.1210/me.2009-0265. [PubMed: 19965929]
8. Brunet A, et al. Protein kinase SGK mediates survival signals by phosphorylating the forkhead transcription factor FKHRL1 (FOXO3a). Mol Cell Biol. 2001; 21:952–965.10.1128/MCB.21.3.952-965.2001 [PubMed: 11154281]
9. Sakoda H, et al. Differing roles of Akt and serum- and glucocorticoid-regulated kinase in glucose metabolism, DNA synthesis, and oncogenic activity. J Biol Chem. 2003; 278:25802–25807. 10.1074/jbc.M301127200 M301127200 [pii]. [PubMed: 12734207]
10. Wiemuth D, et al. Interaction of serum- and glucocorticoid regulated kinase 1 (SGK1) with the WW-domains of Nedd4-2 is required for epithelial sodium channel regulation. PLoS One. 2010; 5:e12163. e12163 [pii] 10.1371/journal.pone.0012163. [PubMed: 20730100]
11. Fejes-Toth G, Frindt G, Naray-Fejes-Toth A, Palmer LG. Epithelial Na+ channel activation and processing in mice lacking SGK1. Am J Physiol Renal Physiol. 2008; 2942007:F1298–1305. 00579.2007 [pii] 10.1152/ajprenal.00579. [PubMed: 18385268]
12. Wu C, et al. Induction of pathogenic T17 cells by inducible salt-sensing kinase SGK1. Nature. 2013 10.1038/nature11984 nature11984 [pii].
13. Kleinewietfeld M, et al. Sodium chloride drives autoimmune disease by the induction of pathogenic T17 cells. Nature. 2013 10.1038/nature11868 nature11868 [pii].
14. Zoncu R, Efeyan A, Sabatini DM. mTOR: from growth signal integration to cancer, diabetes and ageing. Nat Rev Mol Cell Biol. 2011; 12:21–35. nrm3025 [pii] 10.1038/nrm3025. [PubMed: 21157483]
15. Powell JD, Pollizzi KN, Heikamp EB, Horton MR. Regulation of Immune Responses by mTOR. Annu Rev Immunol. 2012; 30:39–68.10.1146/annurev-immunol-020711-075024 [PubMed: 22136167]
16. Delgoffe GM, et al. The mTOR kinase differentially regulates effector and regulatory T cell lineage commitment. Immunity. 2009; 30:832–844. S1074-7613(09)00237-4 [pii] 10.1016/j.immuni.2009.04.014. [PubMed: 19538929]
17. Zhang S, et al. Constitutive reductions in mTOR alter cell size, immune cell development, and antibody production. Blood. 2011; 117:1228–1238. 10.1182/blood-2010-05-287821blood-2010-05-287821 [pii]. [PubMed: 21079150]
18. Delgoffe GM. The kinase mTOR regulates the differentiation of helper T cells through the selective activation of signaling by mTORC1 and mTORC2. Nat Immunol. 2011; 12:295–303. ni.2005 [pii] 10.1038/ni.2005. [PubMed: 21358638]
19. Lee K, et al. Mammalian target of rapamycin protein complex 2 regulates differentiation of Th1 and Th2 cell subsets via distinct signaling pathways. Immunity. 2010; 32:743–753. S1074-7613(10)00205-0 [pii] 10.1016/j.immuni.2010.06.002. [PubMed: 20620941]
20. Murray JT, et al. Exploitation of KESTREL to identify NDRG family members as physiological substrates for SGK1 and GSK3. Biochem J. 2004; 384:477–488. BJ20041057 [pii] 10.1042/BJ20041057. [PubMed: 15461589]
21. Lu M, Wang J, Ives HE, Pearce D. mSIN1 protein mediates SGK1 protein interaction with mTORC2 protein complex and is required for selective activation of the epithelial sodium channel. J Biol Chem. 2011; 286:30647–30654. 10.1074/jbc.M111.257592.M111.257592 [pii]. [PubMed: 21757730]
22. Feldman ME, et al. Active-site inhibitors of mTOR target rapamycin-resistant outputs of mTORC1 and mTORC2. PLoS Biol. 2009; 7:e38. 10.1371/journal.pbio.100003808-PLBI-RA-4959 [pii]. [PubMed: 19209957]
23. Sarbassov DD, Guertin DA, Ali SM, Sabatini DM. Phosphorylation and regulation of Akt/PKB by the rictor-mTOR complex. Science. 2005; 307:1098–1101. [PubMed: 15718470]

24. Guertin DA, et al. Ablation in mice of the mTORC components raptor, rictor, or mLST8 reveals that mTORC2 is required for signaling to Akt-FOXO and PKCalpha, but not S6K1. Dev Cell. 2006; 11:859–871. S1534-5807(06)00459-X [pii] 10.1016/j.devcel.2006.10.007. [PubMed: 17141160]
25. Jacinto E, et al. SIN1/MIP1 maintains rictor-mTOR complex integrity and regulates Akt phosphorylation and substrate specificity. Cell. 2006; 127:125–137. S0092-8674(06)01147-0 [pii] 10.1016/j.cell.2006.08.033. [PubMed: 16962653]
26. Oliver PM, et al. Ndfip1 protein promotes the function of itch ubiquitin ligase to prevent T cell activation and T helper 2 cell-mediated inflammation. Immunity. 2006; 25:929–940. S1074-7613(06)00509-7 [pii] 10.1016/j.immuni.2006.10.012. [PubMed: 17137798]
27. Fang D, et al. Dysregulation of T lymphocyte function in itchy mice: a role for Itch in TH2 differentiation. Nat Immunol. 2002; 3:281–287. 10.1038/ni763 ni763 [pii]. [PubMed: 11828324]
28. Li B, Tournier C, Davis RJ, Flavell RA. Regulation of IL-4 expression by the transcription factor JunB during T helper cell differentiation. EMBO J. 1999; 18:420–432.10.1093/emboj/18.2.420 [PubMed: 9889198]
29. Huang TJ, et al. Allergen-specific Th1 cells counteract efferent Th2 cell-dependent bronchial hyperresponsiveness and eosinophilic inflammation partly via IFN-gamma. J Immunol. 2001; 166:207–217. [PubMed: 11123294]
30. Liu C, et al. Control of beta-catenin phosphorylation/degradation by a dual-kinase mechanism. Cell. 2002; 108:837–847. S0092867402006852 [pii]. [PubMed: 11955436]
31. Yu Q, Sharma A, Sen JM. TCF1 and beta-catenin regulate T cell development and function. Immunol Res. 2010; 47:45–55.10.1007/s12026-009-8137-2 [PubMed: 20082155]
32. Yu Q, et al. T cell factor 1 initiates the T helper type 2 fate by inducing the transcription factor GATA-3 and repressing interferon-gamma. Nat Immunol. 2009; 10:992–999. ni.1762 [pii] 10.1038/ni.1762. [PubMed: 19648923]
33. Roose J, et al. Synergy between tumor suppressor APC and the beta-catenin-Tcf4 target Tcf1. Science. 1999; 285:1923–1926. 7843 [pii]. [PubMed: 10489374]
34. Quezada SA, et al. Tumor-reactive CD4(+) T cells develop cytotoxic activity and eradicate large established melanoma after transfer into lymphopenic hosts. J Exp Med. 2010; 207:637–650. 10.1084/jem.20091918 jem.20091918 [pii]. [PubMed: 20156971]
35. Suissa S, Ernst P, Benayoun S, Baltzan M, Cai B. Low-dose inhaled corticosteroids and the prevention of death from asthma. N Engl J Med. 2000; 343:332–336.10.1056/NEJM200008033430504 [PubMed: 10922423]
36. Fanta CH. Asthma. N Engl J Med. 2009; 360:1002–1014. 10.1056/NEJMra0804579 360/10/1002 [pii]. [PubMed: 19264689]
37. Littenberg B, Gluck EH. A controlled trial of methylprednisolone in the emergency treatment of acute asthma. N Engl J Med. 1986; 314:150–152.10.1056/NEJM198601163140304 [PubMed: 3510384]
38. Sherk AB. Development of a small-molecule serum- and glucocorticoid-regulated kinase-1 antagonist and its evaluation as a prostate cancer therapeutic. Cancer Res. 2008; 68:7475–7483. 10.1158/0008-5472.CAN-08-1047 68/18/7475 [pii]. [PubMed: 18794135]
39. Ackermann TF. EMD638683, a novel SGK inhibitor with antihypertensive potency. Cell Physiol Biochem. 2011; 28:137–146. 10.1159/000331722 000331722 [pii]. [PubMed: 21865856]
40. Kumar A, et al. Muscle-specific deletion of rictor impairs insulin-stimulated glucose transport and enhances Basal glycogen synthase activity. Mol Cell Biol. 2008; 28:61–70. MCB.01405-07 [pii] 10.1128/MCB.01405-07. [PubMed: 17967879]
41. Daan de Boer J, et al. Lipopolysaccharide inhibits Th2 lung inflammation induced by house dust mite allergens in mice. Am J Respir Cell Mol Biol. 2013; 48:382–389. 10.1165/rcmb.2012-0331OCrcmb.2012-0331OC [pii]. [PubMed: 23239494]

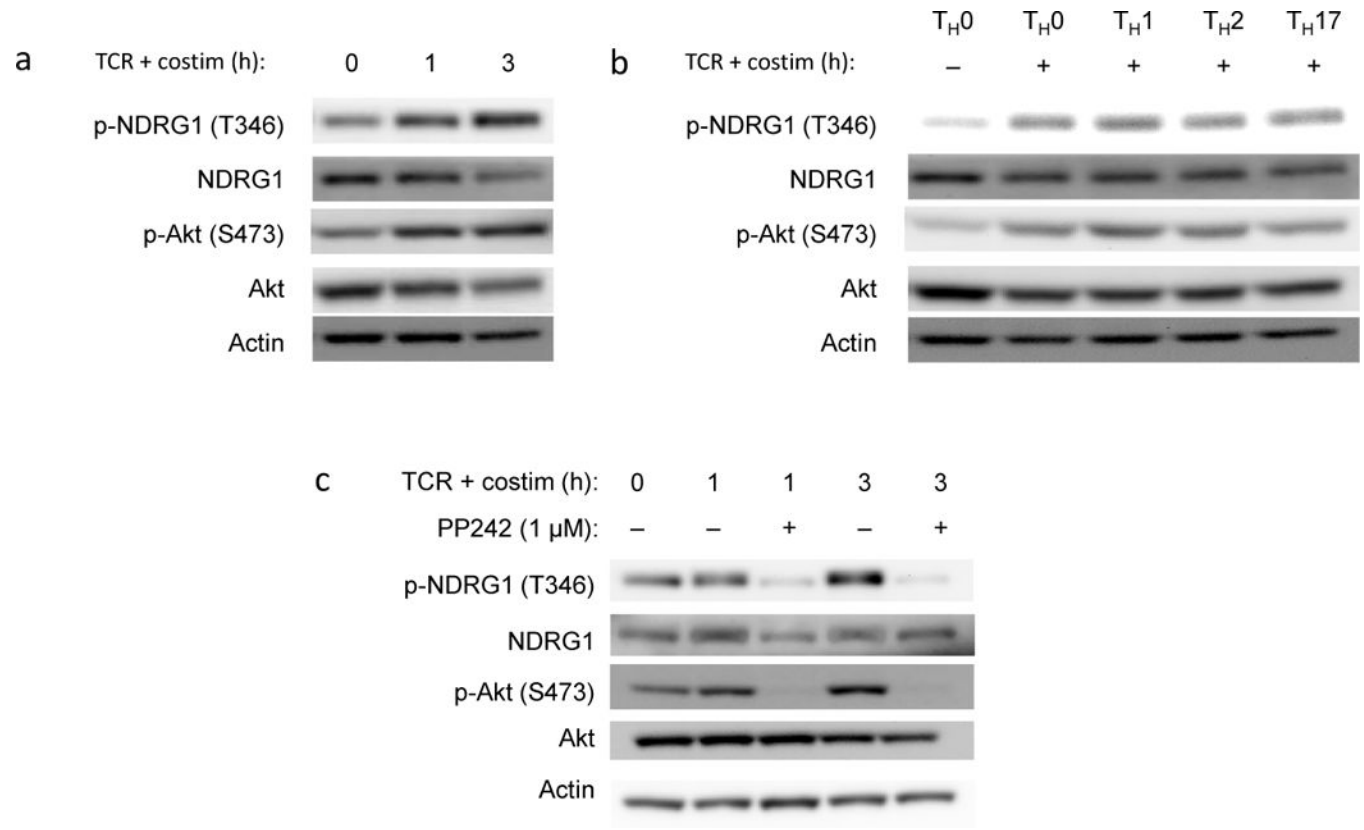

Figure 1. SGK1 is activated downstream of TCR signaling in an mTOR-dependent manner

(a) Immunoblot (IB) of naïve lymphocytes from 5C.C7 mice that were rested for 1 h prior to stimulation with anti-CD3 and anti-CD28. Cells were lysed, and the activity of SGK1 was measured by blotting for phosphorylated NDRG1 (p-T346). The activity of mTORC2 was measured by blotting for phosphorylated Akt (p-S473). Total protein and actin are included as loading controls. **(b)** IB of $CD4^+$ T cells isolated from 5C.C7 mice, as described in a, and stimulated for 3 h in the presence of polarizing cytokines. Cells were lysed and immunoblotted for SGK1 and Akt activity. **(c)** IB of naïve 5C.C7 lymphocytes, as described above. Where indicated, the mTOR kinase inhibitor PP242 (1 μM) was added to the cells upon stimulation. Total protein and actin are included as loading controls. Data are representative of 3–5 independent experiments **(a–c)**.

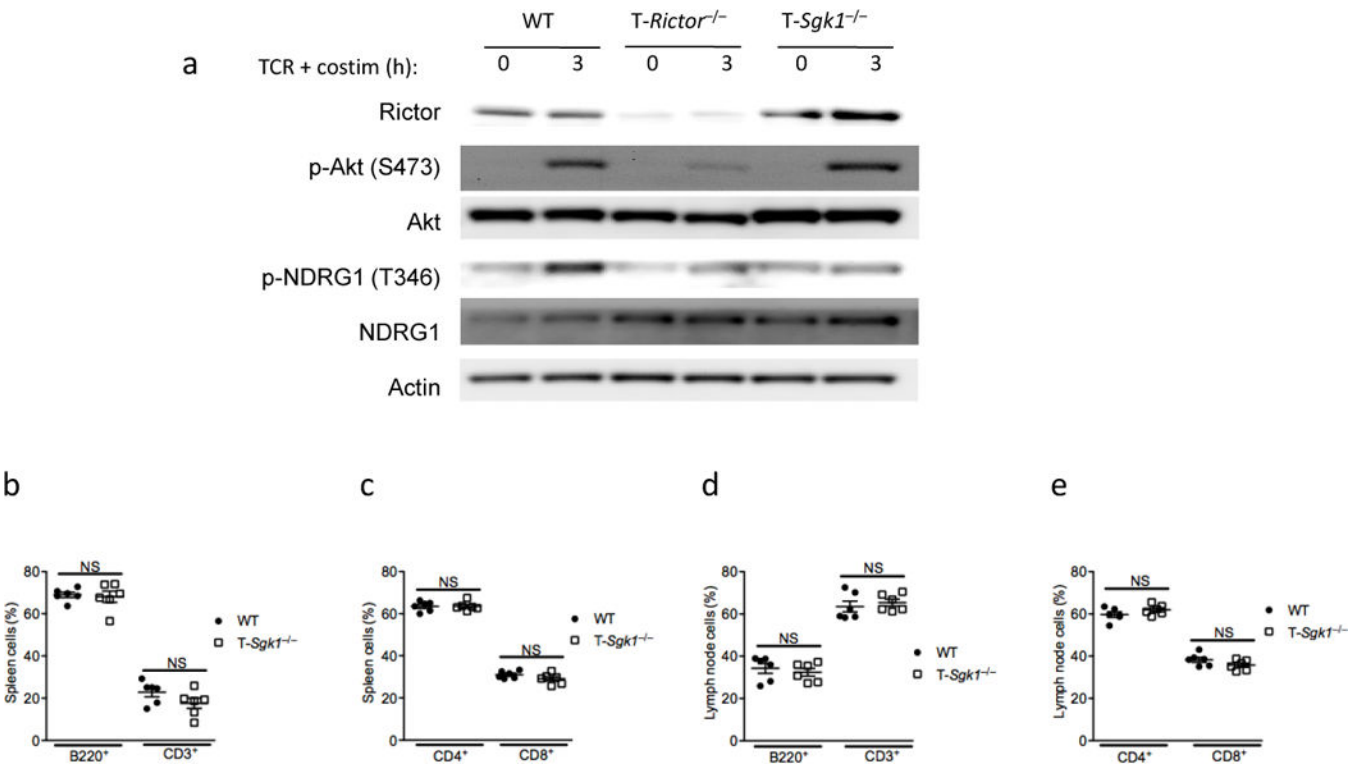

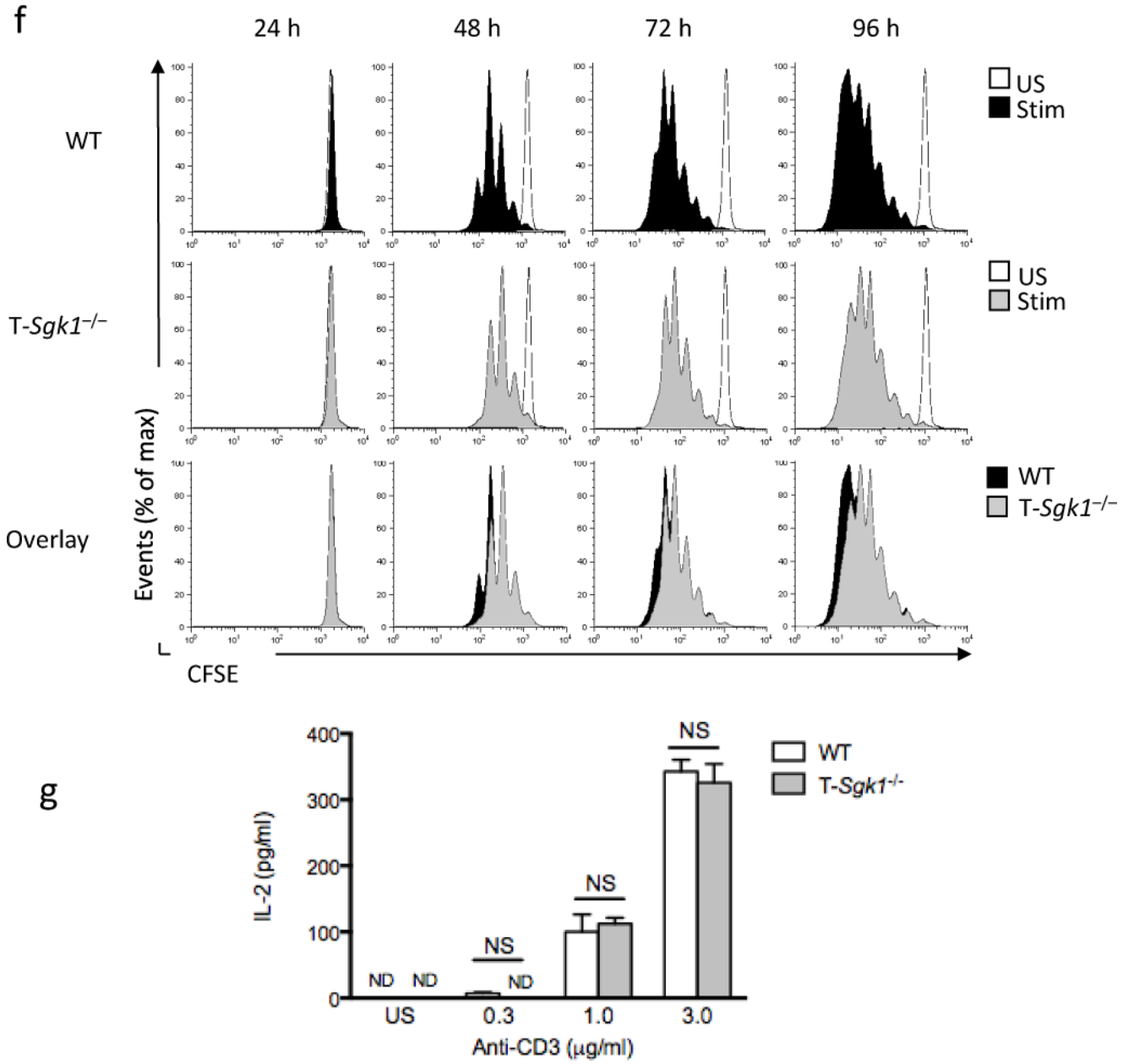

Figure 2. SGK1 is activated downstream of mTORC2 in T cells

(a) IB of wild-type (WT), T-*Rictor*$^{-/-}$, and T-*Sgk1*$^{-/-}$ CD4^{+} T cells that were stimulated as in Fig. 1a. Cells were lysed and the activity of Akt and SGK1 was measured as above. Total protein and actin are included as loading controls. **(b–e)** Flow cytometric phenotyping data compiled from multiple mice (n = 6) showing percentages of B220^{+}, CD3^{+}, CD4^{+} and CD8^{+} cells from WT and T-*Sgk1*$^{-/-}$ spleen (b–c) and lymph nodes (d–e). CD4+ and CD8+ subsets in (c) and (e) were gated on CD3^{+}. **(f)** CD4^{+} T cells were isolated from WT or T-*Sgk1*$^{-/-}$ mice, stained with carboxyfluorescein succinimidyl ester (CFSE), and stimulated with irradiated syngeneic APCs and 1 μg/mL anti-CD3 for 24, 48, 72 or 96 h. Unstimulated (US) cells are shown as a control. **(g)** Naïve CD4^{+} T cells were isolated and stimulated overnight with 0.3, 1.0, or 3.0 μg/ml plate-bound anti-CD3 and 2.0 μg/ml soluble anti-CD28.

Supernatants were harvested to determine IL-2 production by ELISA. ND = not detectable. Data are representative of 3 independent experiments **(a–g)** and samples were analyzed in triplicate in each experiment **(g)**. Statistical significance determined by Student's *t*-test, NS=No Significance, error bars s.e.m.

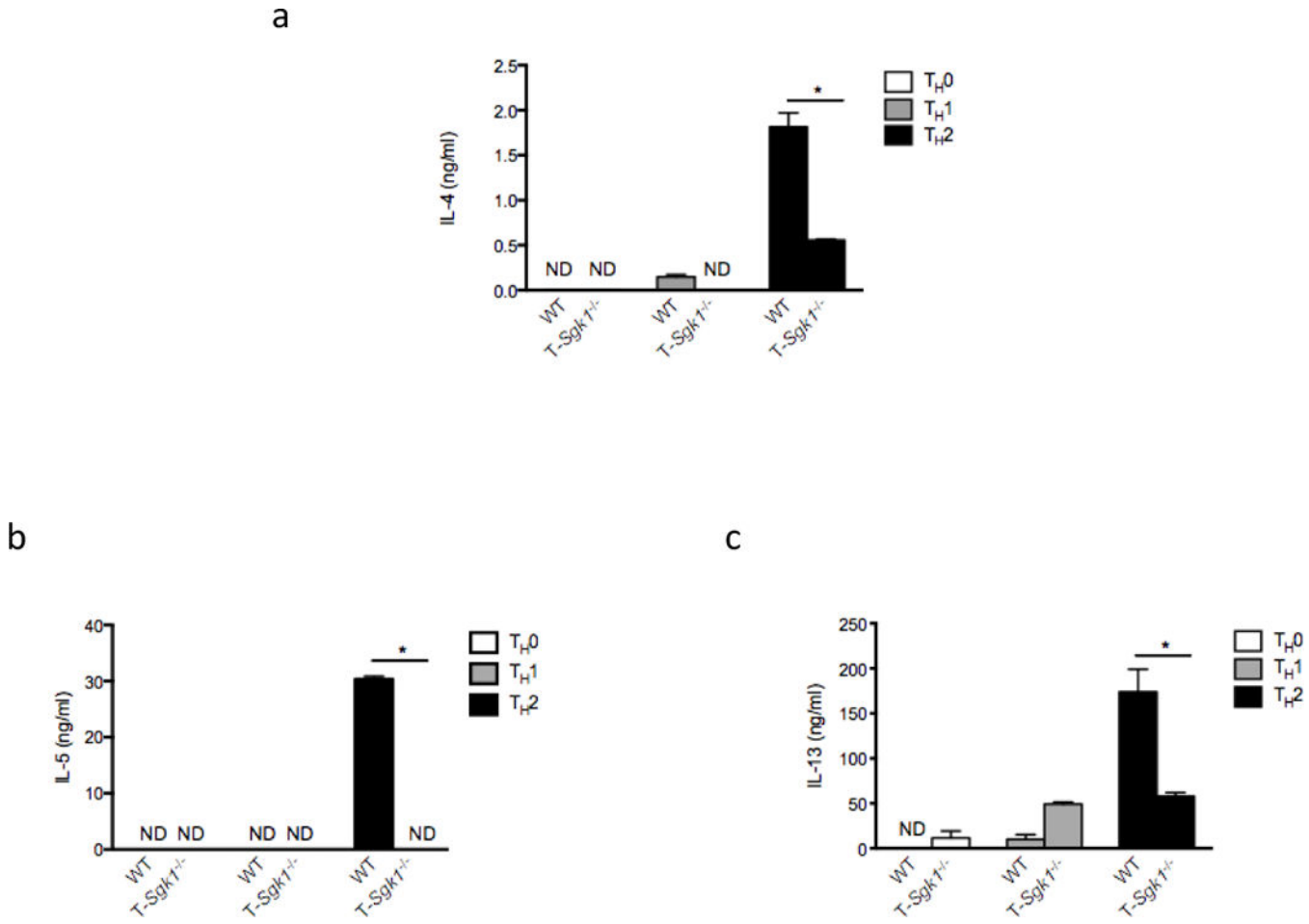

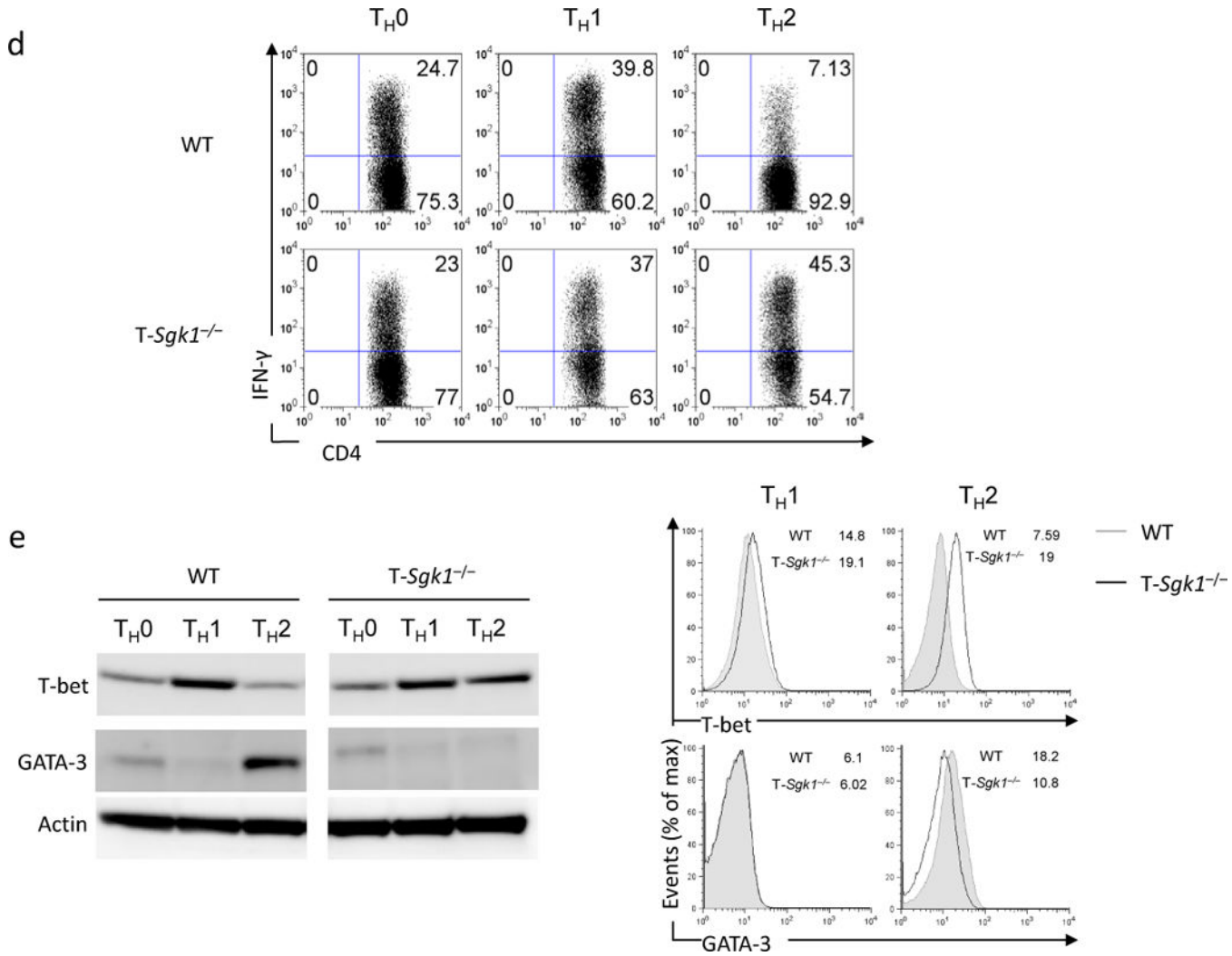

Figure 3. SGK1 reciprocally regulates T_H1 and T_H2 differentiation downstream of mTORC2

(a) IL-4 production of activated CD4$^+$ T cells by ELISA. Naïve CD4$^+$ T cells from WT and T-*Sgk1*$^{-/-}$ mice were isolated based on expression of CD44 and CD62L. Cells were stimulated with irradiated autologous APCs under T_H0, T_H1 or T_H2 polarizing conditions as indicated in the **Methods**. **(b,c)** As in **a**, but supernatants were assayed for IL-5 **(b)** or IL-13 **(c)** production by ELISA. (Statistical significance calculated by ANOVA, **P* < 0.001, error bars s.e.m.) **(d)** IFN-γ production of activated CD4$^+$ T cells by intracellular staining. Cells were stimulated and rested as in **a** prior to activation with overnight plate-bound anti-CD3 and soluble anti-CD28 in the presence of Golgi plug. Numbers represent percentages of cells in each quadrant. **(e)** IB of activated CD4$^+$ T cells for lineage-specific transcription factors. Cells were stimulated with plate-bound anti-CD3 and anti-CD28 for 48 h then rested for 5 days in IL-2. Live cells were harvested, lysed and immunoblotted for T-bet and GATA-3. Actin is included as a loading control. Right, flow cytometric data showing intracellular staining for the transcription factors T-bet and GATA-3. Cells were fixed and permeabilised to determine expression of T-bet and GATA-3 by flow cytometry. Mean Fluorescence Intensity (MFI) is displayed on each respective flow plot. Data are representative of 4

independent experiments **(a–e)** and samples were analyzed in triplicate in each experiment **(a–c)**.

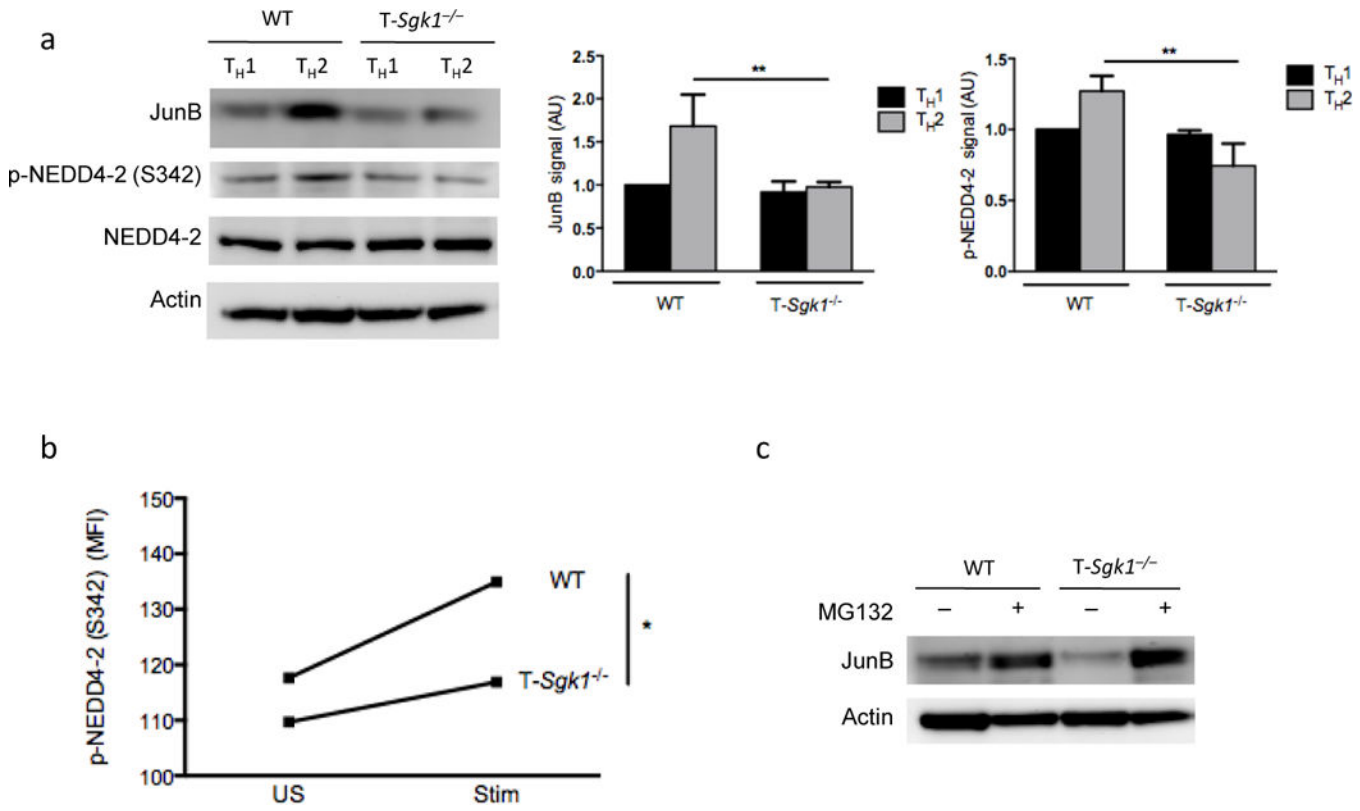

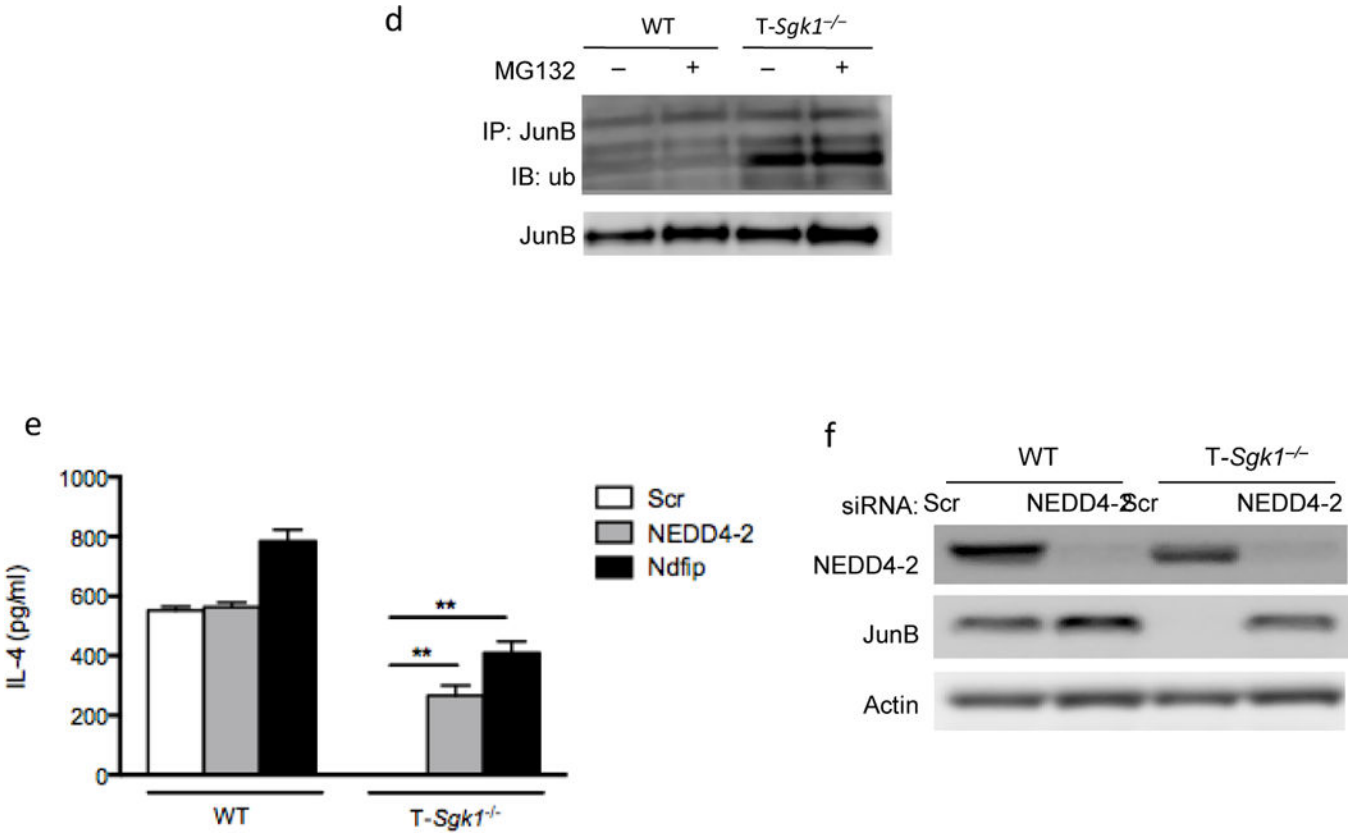

Figure 4. SGK1 promotes Th2 differentiation by negatively regulating NEDD4-2

(a) IB of cell extracts from WT and T-*Sgk1*$^{-/-}$ CD4^{+} T cells that were stimulated *in vitro* under either T_H1 or T_H2 polarizing conditions. Cells were lysed and blotted for the expression of JunB and the activity of the E3 ligase NEDD4-2 (by measuring p-S342). Total NEDD4-2 and actin are included as loading controls. ImageJ software was used to calculate band density from 3 independent experiments, and band density was normalized to loading controls and to WT T_H1 conditions. (Statistical significance calculated by ANOVA, $^{**}P < 0.001$, error bars s.e.m.) **(b)** Intracellular staining of Thy1.1^{+} adoptively transferred cells for phosphorylated NEDD4-2. OT-II CD4^{+} T cells bearing the Thy1.1 congenic marker were adoptively transferred into WT Thy1.2^{+} recipients immunized with OVA adsorbed onto alum to induce a Th2 immune response. Spleens were harvested on day 4, restimulated with OVA Class II peptide, and intracellular staining was performed for phosphorylated NEDD4-2. Plots depict MFI of indicated samples. (Statistical significance calculated by ANOVA, $^{*}P = 0.0183$. **(c)** IB of cell extracts of WT and T-*Sgk1*$^{-/-}$ treated with MG132. Cells were polarized under T_H2 conditions as in **a**, but with the addition of the proteasome inhibitor MG132 during the final 2 h of stimulation. Lysates were blotted for JunB, and actin is included as a loading control. **(d)** Immunoprecipitates (IPs) of JunB from WT and T-*Sgk1*$^{-/-}$ CD4^{+} T cells polarized with IL-4 and treated with MG132. As in **c**, but lysates were subject to IP with JunB antibody. IPs were blotted for ubiquitin and immunoprecipitated JunB is included as a loading control. **(e)** IL-4 production of CD4^{+} T cells transfected with siRNA targeting NEDD4-2 or Ndfip. A non-specific pool of siRNA (scrambled, Scr) was used as a control. Cells were stimulated under T_H2 polarizing conditions for 48 h prior to

transfection with siRNA then expanded in IL-2 for 5 d. Cells were restimulated overnight with anti-CD3 and anti-CD28 and supernatants were harvested to determine cytokine production. **(f)** $CD4^+$ T cells from WT or T-$Sgk1^{-/-}$ mice were treated as in **(e)** then lysed for immunoblot to show knockdown of NEDD4-2 and rescue of JunB protein. (Data not shown for Ndfip.) (Statistical significance calculated by ANOVA, $^{**}P < 0.001$, error bars s.e.m.) Data are representative of 3 independent experiments **(a–d)**, 4 independent experiments **(e)** or 2 independent experiments **(f)**.

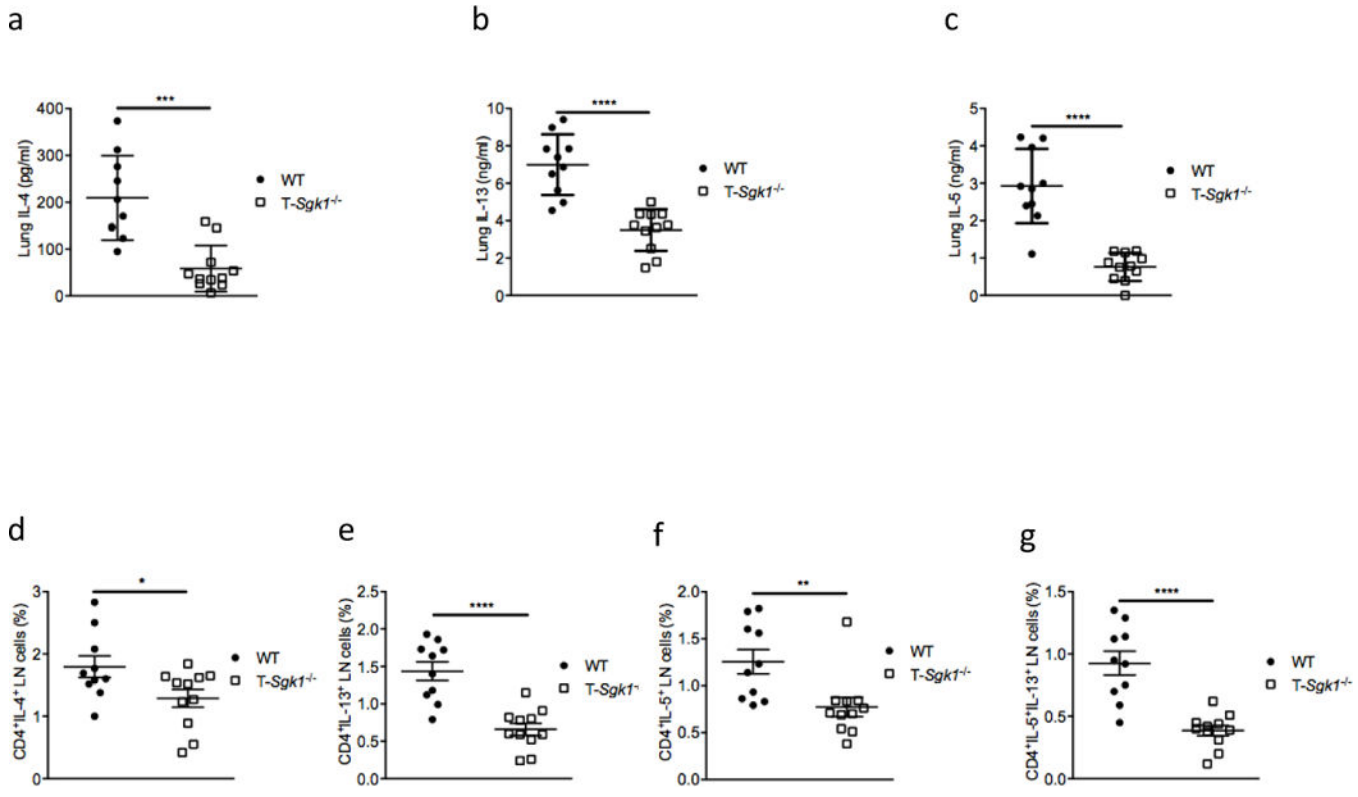

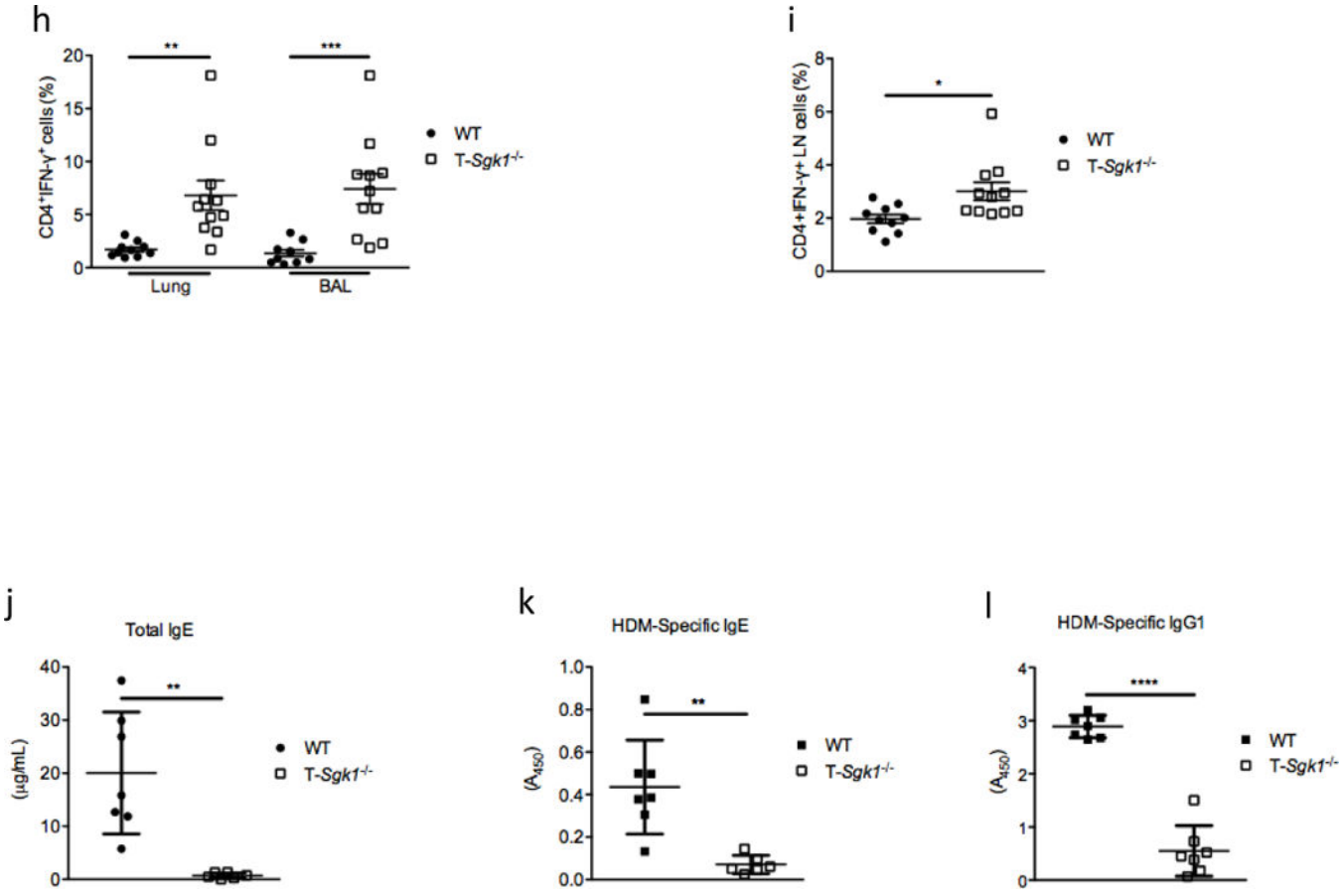

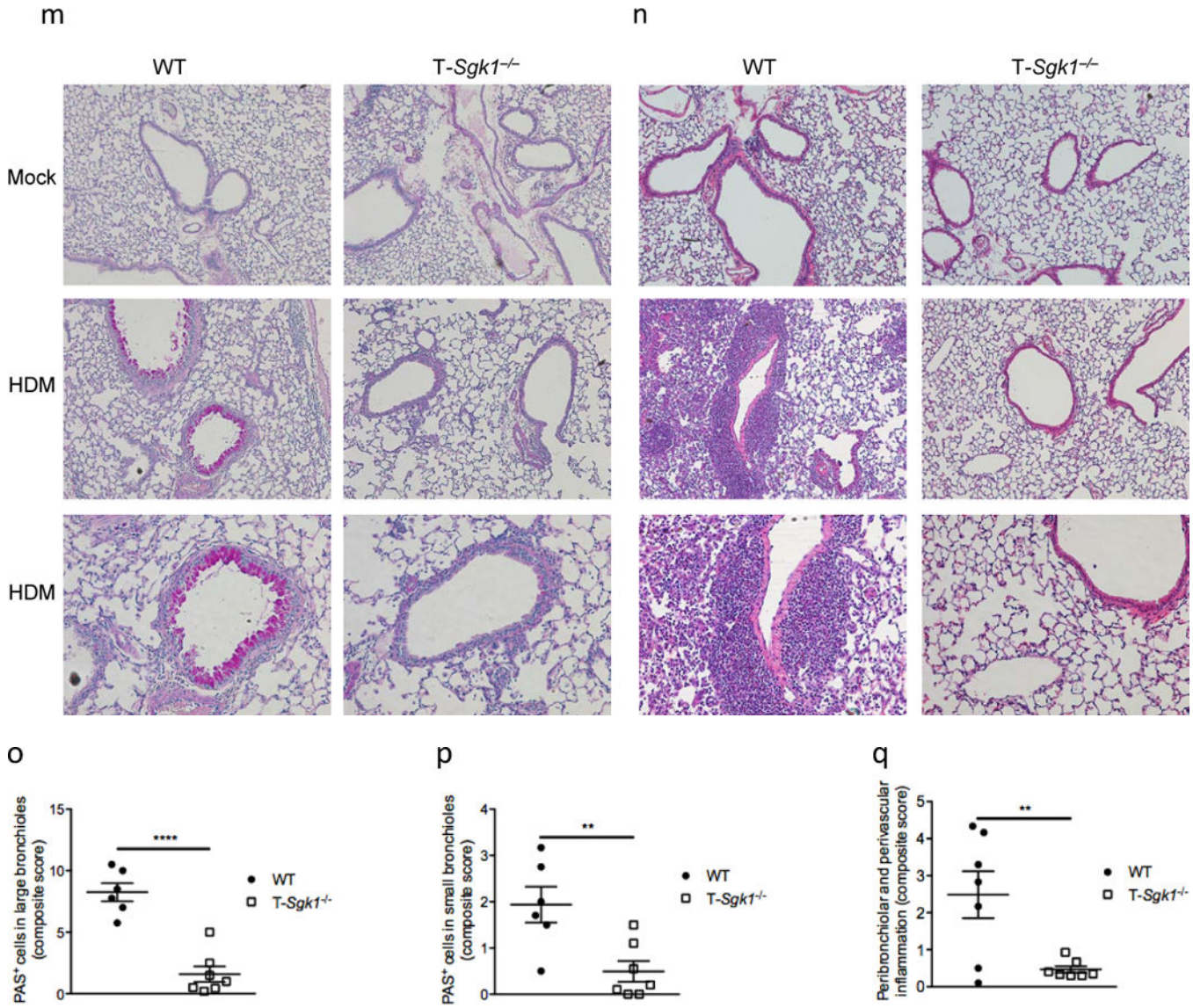

Figure 5. Loss of SGK1 activity in CD4$^+$ T cells mitigates T_H2-mediated disease in an allergen induced asthma model. (a–c)

IL-4, IL-13 and IL-5 production from lung lymphocytes from mice that had been sensitized intraperitoneally and re-challenged intranasally on days 14 and 21 with HDM extract to induce allergic airway inflammation. Lung lymphocytes were stimulated for 3 days *ex vivo* with HDM extract, and supernatants were harvested and analyzed by ELISA for cytokine production. **(d–g)** IL-4, IL-13 and IL-5 production from mediastinal lymph nodes from mice that had been immunized as in **a–c**. Lymphocytes were stimulated *ex vivo* with PMA and ionomycin for 4 h, then fixed, permeabilised and analyzed by intracellular staining and flow cytometry for cytokine production. **(h)** Lymphocytes were harvested from lung parenchyma or BAL, stimulated *ex vivo* with PMA and ionomycin for 4 h, and analyzed for production of IFN-γ by intracellular staining and flow cytometry as described above. **(i)** As in **h**, but lymphocytes were harvested from mediastinal lymph nodes. **(j–l)** Total IgE **(j)**, HDM specific IgE **(k)**, and HDM specific IgG1 **(l)** in serum from mice that were sensitized and

rechallenged with HDM extract as described above. Antibody titers were extrapolated from a standard curve (if available) or absorbance is shown for a dilution of serum for which all samples were in the range of the assay. **(m,n)** Representative lung sections after periodic acid-Schiff (PAS) (m) or hematoxylin and eosin (H&E) (n) staining for saline control (mock) and HDM-treated mice. Pathologic changes in WT mice include goblet cell hyperplasia **(m)** and perivascular and peribronchiolar inflammation **(n)**. Images from HDM treated mice are shown at 10× (top, middle rows) and at 20× magnification (bottom row). **(o–p)** Histologic scoring data of PAS^+ cells in large bronchioles **(o)** and small bronchioles **(p)** from HDM-treated mice. **(q)** Histologic scoring data of perivascular and peribronchiolar inflammation as seen in H&E stained lung sections as described above. Data are representative of 3 independent experiments (a–i), 4 independent experiments (j–l) or 2 independent experiments (m–q), $n = 5–11$ mice per group. (Statistical significance determined by Student's *t*-test (a-q), **** $P < 0.0001$, *** $P < 0.001$, ** $P < 0.01$, * $P < 0.05$, error bars s.e.m.)

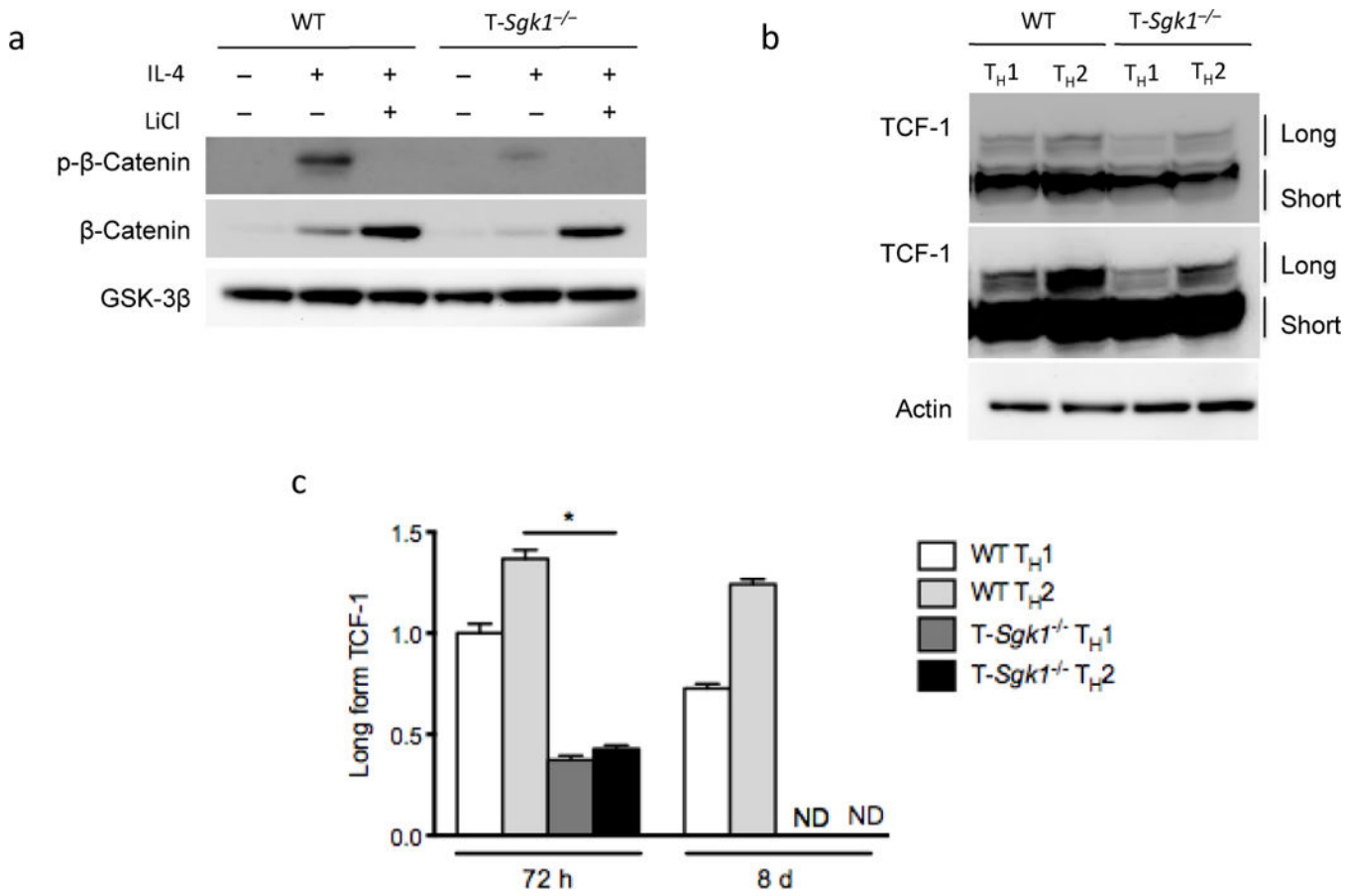

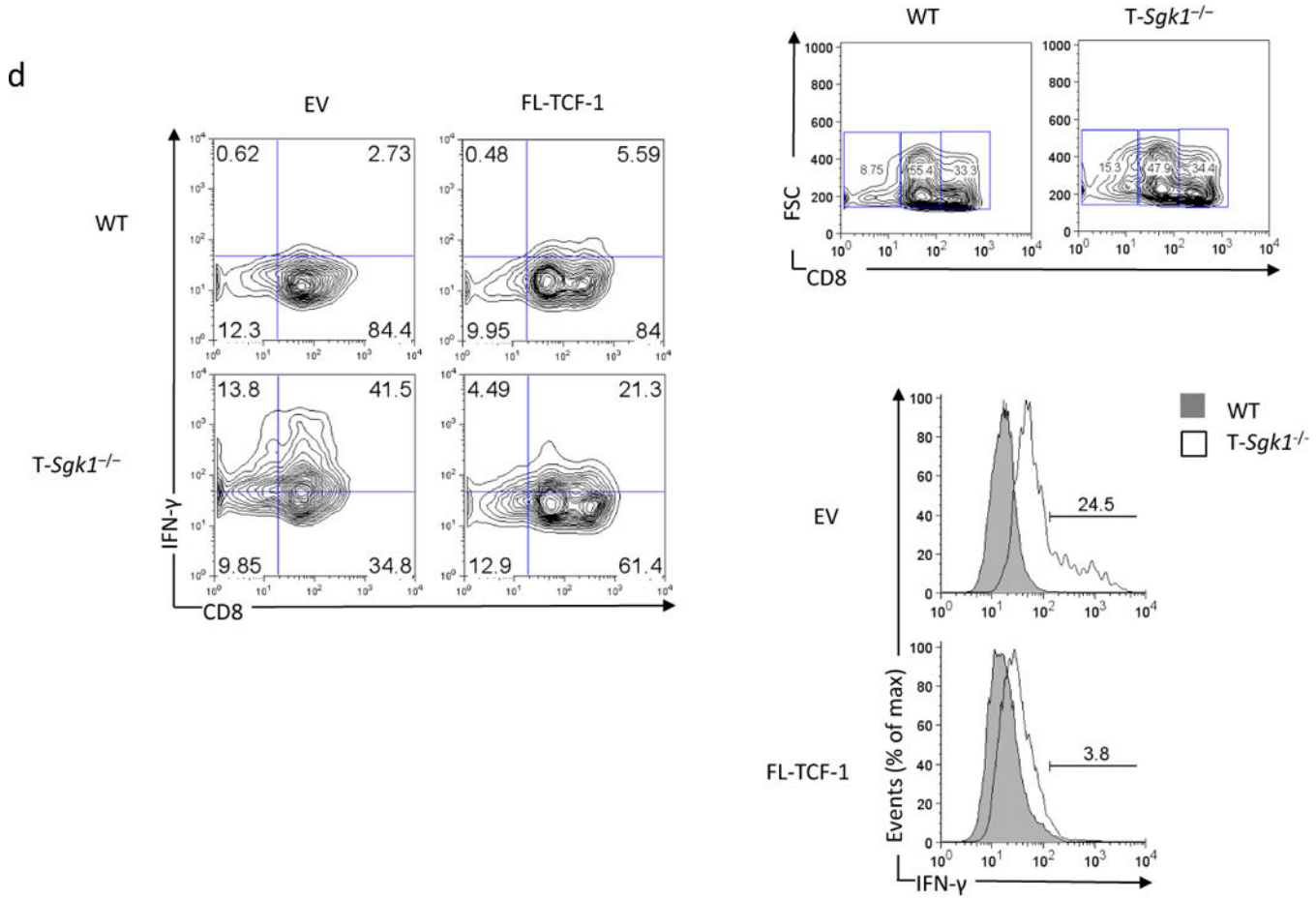

Figure 6. SGK1 negatively regulates T_H1 differentiation via the long isoform of TCF-1

(a) IB of cell extracts from WT and T-*Sgk1*$^{-/-}$ $CD4^+$ T cells stimulated under T_H2 polarizing conditions and treated overnight with 25 mM LiCl. Lysates were blotted for p-β-catenin (S33/47/T41) and total β-catenin. Total GSK-3β is included as a loading control. **(b)** IB of cell extracts from WT and T-*Sgk1*$^{-/-}$ $CD4^+$ T cells that were stimulated *in vitro* under either T_H1 or T_H2 polarizing conditions. Cells were lysed and blotted for TCF-1. Actin is included as a loading control. Two exposures are shown to appreciate differences in long and short isoforms of TCF-1, short exposure (top), long exposure (bottom). **(c)** Expression of long isoform of TCF-1 in activated $CD4^+$ T cells at early and late time points during differentiation. $CD4^+$ T cells were purified from WT and T-*Sgk1*$^{-/-}$ mice by magnetic separation, stimulated with anti-CD3 anti-CD28 magnetic beads for 2 d in T_H1 or T_H2 conditions then rested in IL-2 for 6 d. Fold induction of long isoform of TCF-1 normalized 18S rRNA and to WT T_H1 polarizing conditions at 72 h and 8 days post stimulation, as analyzed by quantitative polymerase chain reaction. **(d)** Flow cytometric analysis of $CD4^+$ T cells polarized under T_H2 conditions and transduced to overexpress the long isoform of TCF-1 (FL-TCF-1) with an MSCV retrovirus containing a human CD8 marker. Following transduction, cells were rested then sorted for human CD8 surface expression. Cells were restimulated and analyzed for production of IFN-© by intracellular staining. Cells were gated on low, intermediate, and high expression of human CD8. Histogram overlays of human CD8 high cells are shown to emphasize differences in IFN-© production among cells

with similar multiplicity of infection. Data are representative of 3 independent experiments **(a–c)** or 4 independent experiments **(d)**, and samples were analyzed in triplicate in each experiment **(c)**. (Statistical significance calculated by ANOVA, $P<0.001$, error bars s.e.m.)

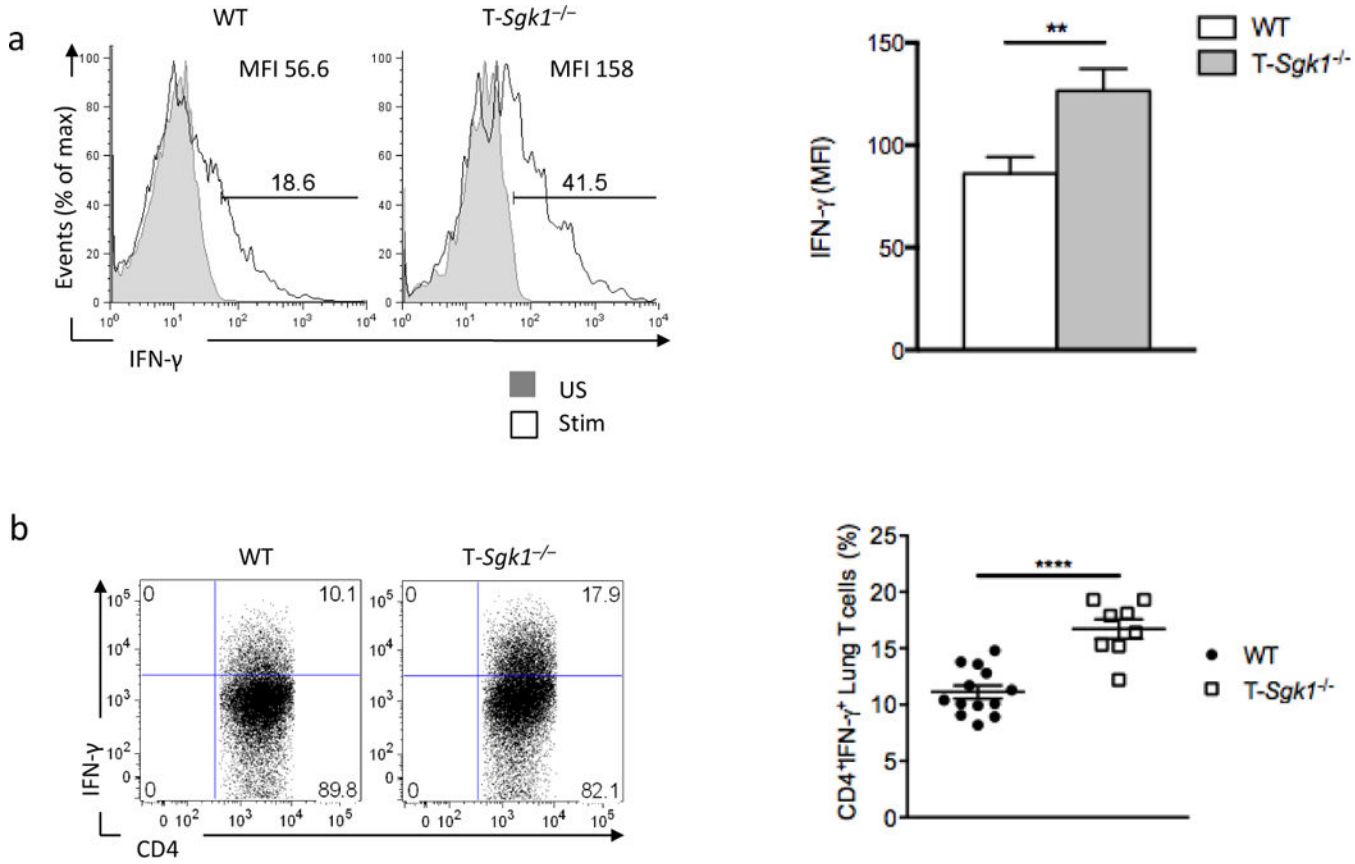

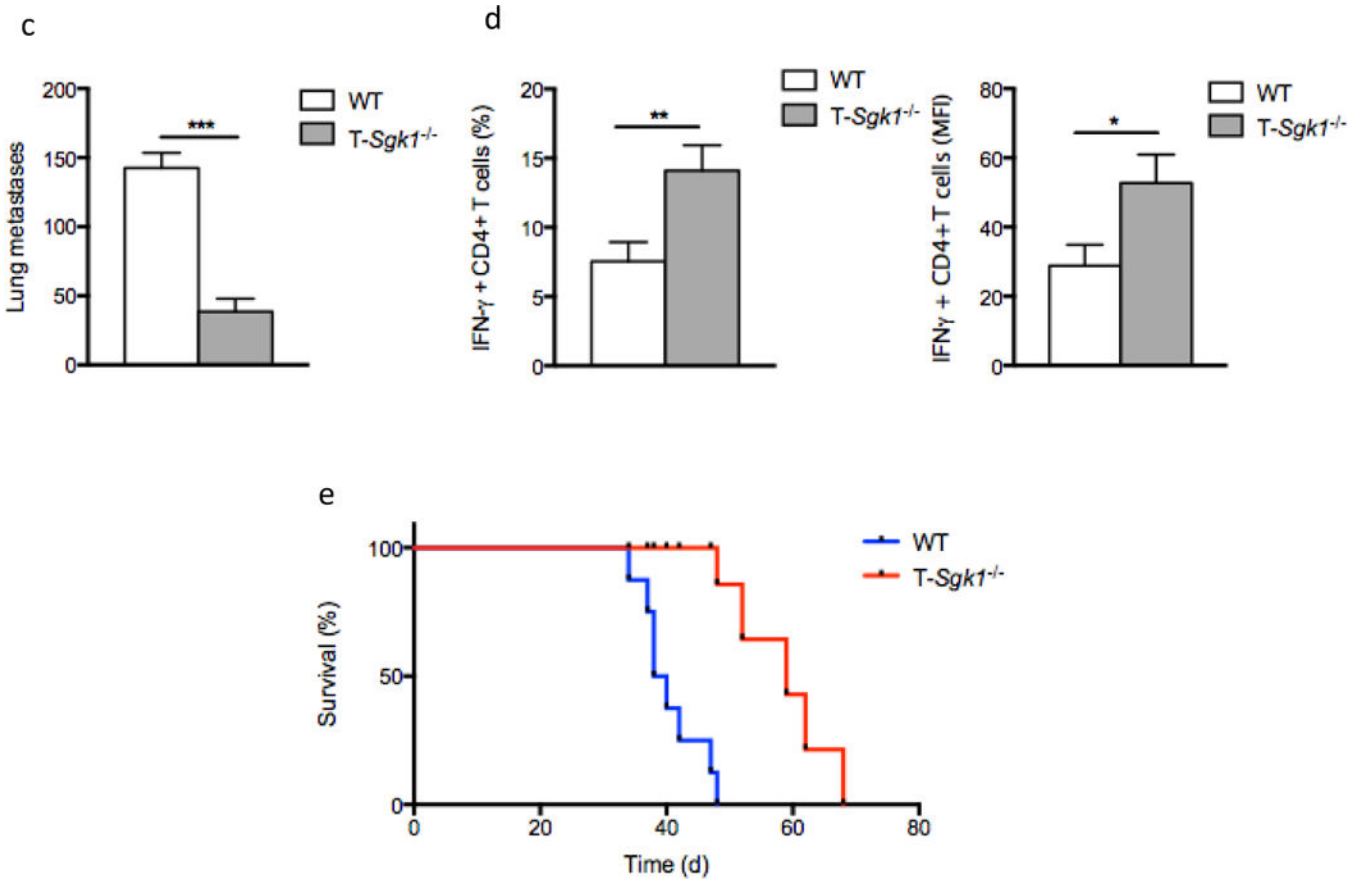

Figure 7. Loss of SGK1 enhances T_H1-mediated viral and tumor immunity

(a) IFN-γ production from adoptively transferred OT-II cells that were restimulated *ex vivo* with PMA and ionomycin. OT-II cells were adoptively transferred into mice that had been simultaneously immunized intravenously with 1×10^6 pfu VAC-OVA. Positive gates for IFN-γ were set using a no stimulation control such that <1.0% of cells were allowed in the positive gate. Plots gated on adoptively transferred cells (left) and bar graph depicts MFI (right). *n* = 10 mice per group. **(b)** IFN-γ production from lung lymphocytes of mice infected intranasally with the PR8 strain of influenza. On day 8, lung lymphocytes were harvested and stimulated for 4 h *ex vivo* with PMA and ionomycin then fixed, permeabilized and analyzed by intracellular staining and flow cytometry for IFN-γ production. **(c)** Number of B16 melanoma lung metastases. WT and T-*Sgk1*$^{-/-}$ mice were injected intravenously with 2×10^5 B16 melanoma cells, and lungs were harvested 21 days later. The number of lung metastases were counted and expressed as mean + s.e.m. **(d)** As in **b**, lung lymphocytes were harvested and stimulated for 4 hours *ex vivo* with PMA and ionomycin and analyzed by intracellular staining for production of IFN-γ by $CD4^+$ T cells. **(e)** Kaplan-Meier analysis of WT and T-*Sgk1*$^{-/-}$ mice vaccinated with 1×10^6 pfu VAC-OVA 7 days prior to challenge with 2×10^5 B16 melanoma cells expressing OVA (B16-OVA). T-*Sgk1*$^{-/-}$ mice have prolonged survival ($P<0.0001$, *n* = 5–7 mice per group). Data are representative of 2–3 independent experiments, *n* = 5–15 mice per group. Statistical significance determined by

Student's *t*-test **(a–d)** or Log-rank (Mantel Cox) survival analysis **(e)**, ****$P < 0.0001$, ***$P < 0.001$, **$P < 0.01$, *$P < 0.05$, error bars s.e.m.